

**NONLINEAR DYNAMICS OF LONGITUDINAL  
GROUND VEHICLE TRACTION**

By

Brian John Olson

A THESIS

Submitted to  
Michigan State University  
in partial fulfillment of the requirements  
for the degree of

MASTER OF SCIENCE

Department of Mechanical Engineering

2001

# ABSTRACT

## NONLINEAR DYNAMICS OF LONGITUDINAL GROUND VEHICLE TRACTION

By

Brian John Olson

The purpose of this study is to investigate and understand the nonlinear dynamics of longitudinal ground vehicle traction. Specifically, the performance of rubber-tired automobiles under straight-ahead braking and acceleration conditions is discussed in detail. Two vehicle-traction models are considered—a quarter-car, or single-wheel model, and a half-car, or two-wheel model—and nonlinear analyses are undertaken for each. Customarily, the forward vehicle speed and the rotational rate of each tire/wheel are taken as dynamic states. This thesis motivates an alternative formulation where wheel slip, a dimensionless measure of the difference between the vehicle speed and the circumferential speed of the tire relative to the wheel center, replaces the angular velocity of the tire/wheel as a dynamic state. This formulation offers new insight into the dynamic behavior of vehicle traction. In each case considered, the unique features of the modeling approach allow one to capture the full range of dynamic responses of the single- and two-wheel traction models in a relatively simple geometric manner. The models developed here may also be useful for developing and implementing ABS and TCS control schemes.

To Julie.

## **ACKNOWLEDGMENTS**

This work was supported in part by the Department of Applied Mechanics at the Budapest University of Technology and Economics, the Department of Mechanical Engineering and the Institute for Global Engineering Education at Michigan State University, the US-Hungarian Joint Fund for Technological Development, and by a grant from the National Science Foundation.

# TABLE OF CONTENTS

<b>LIST OF TABLES</b>	<b>vii</b>
<b>LIST OF FIGURES</b>	<b>viii</b>
<b>1 Introduction</b>	<b>1</b>
1.1 Background . . . . .	2
1.2 Motivation . . . . .	3
1.3 Thesis Organization . . . . .	5
<b>2 The Single-Wheel Braking Model</b>	<b>7</b>
2.1 Tractive Properties . . . . .	9
2.1.1 Wheel Slip . . . . .	9
2.1.2 The Tire/Road Interface and Friction Law . . . . .	10
2.1.3 Friction Characteristic and Tire Model . . . . .	10
2.2 Equations of Motion . . . . .	13
2.2.1 $u$ and $\omega$ as Dynamic States . . . . .	13
2.2.2 The $(u, \omega R)$ Phase Plane . . . . .	14
2.2.3 $u$ and $s$ as Dynamic States . . . . .	17
2.3 Steady-Slip Conditions . . . . .	19
2.4 Local Stability of Slip Dynamics . . . . .	19
2.5 Global Features of the Single-Wheel Braking Model . . . . .	21
2.6 Hysteresis in the Single-Wheel Braking Model . . . . .	25
2.7 The Transition to Unstable Braking . . . . .	25
2.7.1 Lockup Instability . . . . .	26
2.7.2 The Critical Brake Torque . . . . .	27
2.8 The Effects of Aerodynamic Drag and Rolling Resistance . . . . .	28
<b>3 The Single-Wheel Acceleration Model</b>	<b>31</b>
3.1 Equations of Motion . . . . .	32
3.2 Steady-Slip Conditions and Local Stability . . . . .	33
3.3 Global Features of the Single-Wheel Vehicle Acceleration Model . . . . .	34

<b>4</b>	<b>Two-Wheel Braking and Acceleration Models</b>	<b>39</b>
4.1	The Two-Wheel Braking Model . . . . .	39
4.1.1	Equations of Motion . . . . .	41
4.1.2	Steady-Slip Conditions . . . . .	42
4.1.3	Global Features of the Two-Wheel Braking Model . . . . .	46
4.2	The Two-Wheel Acceleration Model . . . . .	48
4.2.1	Equations of Motion . . . . .	48
<b>5</b>	<b>Conclusions and Directions for Future Work</b>	<b>50</b>
	<b>BIBLIOGRAPHY</b>	<b>52</b>

## LIST OF TABLES

2.1	Steady-slip values for the single-wheel braking model . . . . .	22
3.1	Steady slip values for the single wheel acceleration model. . . . .	35

## LIST OF FIGURES

2.1	Schematic of the single-wheel braking model and corresponding free body diagram . . . . .	8
2.2	Typical longitudinal friction characteristics: (a) dry asphalt; (b) wet asphalt; (c) gravel; and (d) packed snow. . . . .	12
2.3	State space descriptions for the single-wheel braking model in the $(u, \omega R)$ state space for $\Psi = 15$ : (a) $\Upsilon_b = 7$ ; (b) $\Upsilon_b = 12$ ; (c) $\Upsilon_b = \Upsilon_{b_{cr}} = 15.250$ ; (d) $\Upsilon_b = 18$ . . . . .	16
2.4	State space descriptions for the single-wheel braking model for $\Psi = 15$ and $\Upsilon_b = 12$ : (a) in $u$ and $\omega R$ ; (b) in $u$ and $s$ . . . . .	17
2.5	$h_b(s)$ vs. $s$ and corresponding state space descriptions in $u$ and $s$ for $\Psi = 15$ : (a) $\Upsilon_b = 7$ ; (b) $\Upsilon_b = 12$ ; (c) $\Upsilon_b = \Upsilon_{b_{cr}} = 15.250$ ; (d) $\Upsilon_b = 18$ . See Table 2.1 for steady slip values. . . . .	23
3.1	Schematic of the single-wheel acceleration model and corresponding free body diagram . . . . .	32
3.2	$h_t(s)$ vs. $s$ and corresponding state space descriptions in $u$ and $s$ for $\Psi = 15$ : (a) $\Upsilon_e = 7.5$ ; (b) $\Upsilon_e = 15.0$ ; (c) $\Upsilon_e = 22.5$ . See Table 3.1 for steady-slip values. . . . .	36
3.3	$h_t(s)$ vs. $s$ and corresponding state space descriptions in $u$ and $s$ in detail near a rapid set of bifurcations: (a) $\Upsilon_e = 14.65$ ; (b) $\Upsilon_e = 15.196$ ; (c) $\Upsilon_e = 15.65$ . See Table 3.1 for steady-slip values. . . . .	37
3.4	$h_t(s)$ vs. $s$ and corresponding state space descriptions in $u$ and $s$ in detail near a rapid set of bifurcations: (d) $\Upsilon_e = 16.032$ ; (e) $\Upsilon_e = 16.65$ . See Table 3.1 for steady-slip values. . . . .	38
4.1	Schematic of the two-wheel braking model and corresponding free body diagram of a single wheel . . . . .	40
4.2	$\Lambda_b(s)$ for $h = 1.25$ , $c = 6$ , $b = 4$ , and $\theta = 0$ . A wet asphalt friction characteristic has been employed. . . . .	42

4.3	The functions (a) $h_{br}(\mathbf{s})$ and (b) $h_{bf}(\mathbf{s})$ for $h = 1.25$ , $c = 6$ , $b = 4$ , $\theta = 0$ , $\Psi = 15$ , $\Upsilon_{br} = 3.5$ , and $\Upsilon_{bf} = 10.0$ . . . . .	43
4.4	(a) The solution sets $\mathcal{S}_i^\pm$ ( $i = r, f$ ) and (b) the corresponding state space description of the slip dynamics of the two-wheel model for $h = 1.25$ , $c = 6$ , $b = 4$ , $\theta = 0$ , $\Psi = 15$ , and $\Upsilon_{br} = 3.5$ , $\Upsilon_{bf} = 10.0$ . . . . .	45
4.5	Qualitative description of the steady-slip conditions for the two-wheel braking model as a function of the brake torques ( $h = 2m$ , $c = 6m$ , $b = 4m$ , $\theta = 0$ , and $\Psi = 15$ ): (I) <i>Stable</i> ; (II) <i>Mixed (Front)</i> ; (III) <i>Mixed (Rear)</i> ; (IV) <i>Mixed (Front &amp; Rear)</i> ; (V) <i>Lockup</i> . Example slip space vector fields in front and rear slip. . . . .	47
4.6	Schematic of the two-wheel vehicle acceleration model and corresponding free body diagram of a single wheel . . . . .	48

# CHAPTER 1

## Introduction

In its most general sense, vehicle dynamics refers to the response due to imposed forces of ground vehicles, aerospace vehicles, aircraft, and marine craft. The latter are supported by a fluid: either air or water. Ground vehicles may be broadly categorized as either guided or nonguided. Guided ground vehicles, such as railway and track-levitated trains, are constrained to move along a fixed path, whereas nonguided vehicles are free to move in any direction on the ground. This thesis investigates the nonlinear dynamics of rubber-tired automobiles—one class of nonguided ground vehicles—with traction under straight-ahead, or longitudinal braking and acceleration conditions. Gillespie [1] or Wong [2] offer good accounts of ground transportation technology and the fundamentals and theory of nonguided ground vehicles.

The dynamics of ground vehicles are often described in terms of performance, handling, and ride. The performance of a vehicle refers to its ability to respond to imposed forces under acceleration or braking conditions and/or in cornering. Thus, vehicle performance is based upon objective properties of the vehicle. The handling of a ground vehicle, however, depends upon the driver/vehicle combination and the ability of the vehicle to respond to driver commands. Ride characteristics include the effects of noise and vibration due to, for example, road roughness, the tire/wheel, driveline or engine, on driver comfort and her or his perception and tolerance to such

excitations.

This work investigates the tractive performance of rubber-tired automobiles under longitudinal braking and acceleration conditions. A general background of these systems is outlined next, followed by the motivation for the present study. The chapter closes with an outline of the thesis organization.

## 1.1 Background

In studies of vehicle traction the gross vehicle dynamics and tire/wheel dynamics can be captured by lumped mass models. Simplified models that are often considered for longitudinal braking and acceleration include the single-wheel model [1, 2, 3], and a two-dimensional, two-wheel model (front and rear) [1, 2], or full four-wheel models for cornering [1, 2]. The dynamics of these systems involve interactions between the vehicle, the tire/wheel assemblies, and the road surface. The force that ultimately slows or accelerates the vehicle is the longitudinal friction force between the road and tire, which can be empirically described in terms of a slip condition at the interface. Thus, writing the equations of motion for any rubber-tire vehicle system requires a description of the friction force generated at the tire/road interface, in addition to the usual laws of motion.

Experimental evidence shows that the longitudinal friction force is proportional to the normal force at the contact [1, 2, 3], with a coefficient of friction serving as the 'constant' of proportionality. This coefficient can be conveniently modeled in an empirical manner that depends on the slip [4, 5], which is a dimensionless measure of the difference between the vehicle speed and the circumferential speed of the tire relative to the wheel center. During braking (resp. acceleration), this difference is generated by a brake (resp. engine) torque on the wheel, which acts against (resp. with) the inertia of the vehicle. The slip depends on the dynamics of the vehicle and

the tire/wheel, and it also influences their dynamics through the friction force. This "feedback" results in a system of coupled equations of motion for the vehicle and the tire/wheel. These equations of motion are most often formulated in terms of the vehicle's speed relative to ground and the absolute rotational rate of the tire/wheel. This is a very natural formulation, wherein the slip is merely an internal variable defined in terms of the system's dynamic states, which is used to compute the friction force that appears in the equations of motion.

## 1.2 Motivation

In this thesis, a formulation is considered in which the slip is taken to be a dynamic state variable, replacing the absolute rotational rate of the tire/wheel speed. Liu and Sun [6] have developed the equations of motion for a quarter-car model in this way, but their investigation focuses on control algorithms based on gain-scheduling, rather than general dynamic behavior. The formulations herein focus not on control, but the performance aspects of vehicle traction. It will be shown that the equations of motion for the single- and two-wheel models take on forms that lend themselves to relatively simple investigation and interpretation using tools from nonlinear dynamics. Specifically, in the single-wheel braking and acceleration models this formulation allows the dynamics for the entire range of vehicle speeds and slip values to be captured by a single function (one for each model) that is defined in terms of the slip, the brake or engine torque, and the friction/slip relationship. These functions describe completely the behavior of a given vehicle during braking (resp. acceleration) and under a constant or slowly varying brake torque (resp. engine torque). Similarly, for each of the two-wheel traction models, a set of two such functions completely capture the dynamics: one each for the front and rear slip states. In each case the phase space of the system can be completely characterized by these functions, thereby providing

a relatively simple means of categorizing different operating regimes.

The dynamic models presented here are capable of describing both transient and steady tractive performance. Most importantly, they clearly demonstrate how a vehicle can undergo stable braking or acceleration and/or lockup, depending on the brake/engine torque, the friction characteristic, and the vehicle parameters. These models also allow one to clearly see how transitions between operating states occur as parameters and conditions are varied. In fact, for the single-wheel models, a single set of phase plane diagrams, drawn at varying brake/engine torque levels, completely captures the entire range of possible behaviors for a given friction characteristic. The two-wheel models are more complicated, but a quite complete picture of the dynamic possibilities is captured in a relatively simple set of diagrams, including various combinations of lockup and stable slip at each tire/wheel. These ideas can be extended to the four-wheel case, for example to analyze traction during cornering, although such studies are not considered here.

One of the more interesting findings of this study is a stability result related to brake lockup. The standard thinking is that the brake torque can increase until the slip reaches a value that corresponds to the maximum coefficient of friction, beyond which lockup occurs [1, 2]. Under steady-state braking conditions the corresponding maximum brake torque is typically assumed to be equal to the peak moment provided by the friction force about the wheel center. In this work it is shown that this result is actually an approximation that is only accurate when the inertia of the tire/wheel is very small compared to that of the vehicle. Since this is generally the case, the approximation works well, but the present results determine where instability to lockup actually occurs and also systematically shows how the approximation is obtained.

The present formulations are useful for describing the important qualitative features of vehicle traction and providing useful insight into stability issues. It is recognized that slip is notoriously difficult to measure in practice, primarily since it is not

a simple matter to determine the vehicle speed relative to ground. (The speedometer uses the tire circumferential speed, which does not match the vehicle speed during slip—and this is precisely when both speeds are required to compute the slip [7].) However, since methods exist for estimating the slip [8, 9, 10], models such as those developed here may be useful for developing and implementing anti-lock brake systems (ABS) and traction control systems (TCS).

### 1.3 Thesis Organization

The thesis is organized as follows. The single-wheel braking model is developed first in a systematic manner, thus laying the necessary groundwork for the development and analysis of a single-wheel acceleration model, and subsequently two-wheel vehicle traction models. The equations of motion are presented and the need to quantify the available friction force for braking is specified. This motivates an investigation of the tire/road interface and leads to the introduction of force coefficient characteristics as a function of longitudinal wheel slip. The equations of motion are hence cast into a framework that is convenient for a nonlinear dynamic analysis. Two formulations are considered: one in which the dynamic states are taken to be the forward vehicle speed and the angular speed of the tire/wheel, and one in which wheel slip replaces the angular speed as a dynamic state. The latter formulation is pursued in detail. Global features of the single-wheel model are discussed, including steady-slip conditions, local stability of slip dynamics, hysteresis, and the transition to unstable braking. The effects of aerodynamic drag and rolling resistance on the resulting nonlinear equations of motion are also considered. A single-wheel acceleration model is similarly developed and analyzed. Finally, the single-wheel braking and acceleration models are extended to half-car, or two-wheel traction models. The two-wheel braking and acceleration models are developed, and the analysis of each follows in much the same

way as their single-wheel counterparts, although the range of possible behaviors is significantly more involved. The thesis closes with conclusions and directions for future work.

# CHAPTER 2

## The Single-Wheel Braking Model

A quarter-car model is developed in this chapter in order to illustrate the fundamental aspects of vehicle braking. This single-wheel model is unrealistic by virtue of its simplicity, and it clearly fails to capture some important dynamical features (e.g., dynamic load transfer). It nevertheless serves to facilitate an understanding of the basic dynamic characteristics of vehicle braking. In fact, the approach taken here lays the groundwork for subsequent formulations, namely, that of the single-wheel acceleration model of Chapter 3, and the two-wheel braking and acceleration models of Chapter 4.

As depicted in Figure 2.1, the quarter-car model consists of a single wheel constrained to move longitudinally in the  $x$ -direction at a speed  $u$  and with a rotational rate  $\omega$ . Denoted by  $R$  and  $J$  are its effective rolling radius and polar moment of inertia, respectively. The effect of a braking mechanism on the vehicle wheel is captured by the brake torque  $T_b$ , which opposes the forward motion of the system. The vertical reaction force  $Z$  balances the static weight  $mg$ , while the longitudinal force  $X$  serves to slow the vehicle in braking. By summing forces in the  $x$ - and  $z$ -directions and moments about the mass center  $C$  of the vehicle/wheel, the system equations are

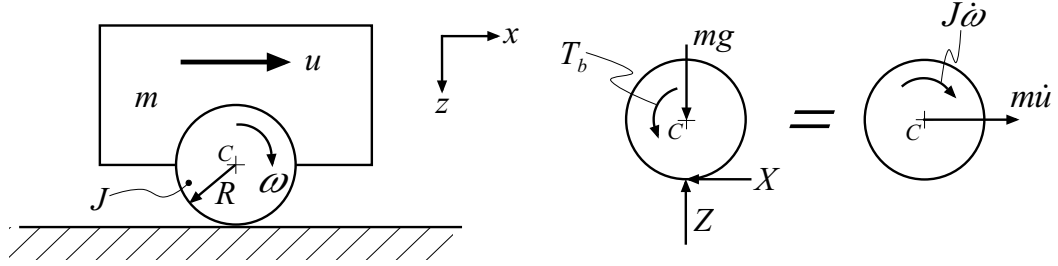


Figure 2.1. Schematic of the single-wheel braking model and corresponding free body diagram

found to be

$$m\dot{u} = -X, \quad (2.1)$$

$$Z = mg, \quad (2.2)$$

$$J\dot{\omega} = RX - T_b, \quad (2.3)$$

where  $m$  is the mass of the vehicle-wheel combination and  $g$  is the acceleration due to gravity. Overdots denote differentiation with respect to time.

In general, there are a number of forces acting on a vehicle that may give rise to a deceleration. The model considered here includes only the longitudinal brake force  $X$ , which is discussed in detail in the next section. Other sources of deceleration in braking include driveline drag, grade, rolling resistance, and aerodynamic drag. Driveline drag refers to the resistance to a change in vehicle velocity due to the inertia of engine and transmission components, and also to bearing and gear friction in the transmission, differential, and engine. Grade is defined as the ratio of a unit vertical to unit horizontal distance and contributes directly—either in the positive (uphill) or negative (downhill) sense—to vehicle deceleration. The effects of grade and driveline drag will not be considered here. Simple models for aerodynamic drag and rolling resistance are incorporated into the equations of motion in Section 2.8.

## 2.1 Tractive Properties

The primary force of interest in studies of vehicle traction is the longitudinal force  $X$ , which acts on the vehicle through a tire/road contact patch. Experimental evidence shows that this friction force is proportional to the normal force  $Z$  at the contact and is a consequence of the relative difference between the vehicle speed  $u$  and the rolling speed of the tire  $\omega R$ . The "constant" of proportionality is responsible for the friction coupling, and can be empirically determined by a friction characteristic in terms of road test data and wheel slip, which is a dimensionless measure of the difference between  $u$  and  $\omega R$ . Since the friction characteristic captures the typifying quantities of a particular tire/road combination—including slip stiffness at zero slip and peak brake force values—it can be regarded as a tire model that characterizes the tire behavior on a given road surface. The tractive properties are now discussed in terms of wheel slip, the tire/road interface and friction law, and a tire model.

### 2.1.1 Wheel Slip

The longitudinal friction force  $X$  is a consequence of the relative difference between the vehicle speed  $u$  and the rolling speed of the tire, which is given by  $\omega R$ . Wheel slip is defined in terms of this difference as\*

$$s \equiv \frac{u - \omega R}{\max(u, \omega R)}. \quad (2.4)$$

It is assumed and taken as convention that  $u > 0$  and  $0 \leq \omega R \leq u$  in vehicle braking. Thus,  $s = \frac{u - \omega R}{u}$  is defined on the unit interval  $I = [0, 1]$ , taking on the limiting values of  $s = 0$  for free rolling ( $u = \omega R$ ) and  $s = 1$  for wheel lockup ( $\omega R = 0$ ). The former

---

\*The maximum function  $\max(u, \omega R)$  allows the use of Equation (2.4) to define longitudinal wheel slip for both vehicle braking and acceleration. In braking  $u > \omega R$ , while  $u < \omega R$  for vehicle acceleration.

case when  $u = \omega R$  implies the absence of a brake torque. The definition of slip, along with the convention that  $\omega R \leq u$  allows for two possibilities for steady-state vehicle braking with nonzero initial speed: (1) finite rotation of the wheel while the vehicle decelerates and (2) deceleration under lockup conditions. It is noted that the latter case of lockup is undesirable since steerability, directional stability, and general control over a vehicle is severely degraded in such a state [1, 2].

### 2.1.2 The Tire/Road Interface and Friction Law

In a rubber tire, wheel slip results in the deformation and sliding of tread elements in the tire/road contact patch, which in turn sustains the friction force  $X$  in braking. Indeed, it is through this important interface between the road surface and tire tread that braking is negotiated. In general, the microscopic physical description of the said phenomenon is complicated and involves more physics than what are needed here. (See, for instance, [1, 2].) It suffices to capture these interactions by the simple algebraic relationship

$$X = \mu(s)Z, \tag{2.5}$$

which is known as the *friction law* or *creep force equation*. The longitudinal force coefficient  $\mu : I \rightarrow I$  is experimentally determined in terms of road test data and is the subject of the next section.

### 2.1.3 Friction Characteristic and Tire Model

The friction coupling between a rubber tire and road surface depends on a number of physical parameters involving tire construction, inflation and wear, the tire/road interface, and vehicle speed and loading [1, 2, 3]. Since a general theory that can accurately predict the longitudinal brake force in terms of wheel slip has yet to be developed, friction coupling is necessarily determined experimentally. Various methods

exist to relate the brake and normal forces  $X$  and  $Z$  in terms of a friction characteristic  $\mu(s)$ . See, for example, [9, 8]. The resulting data can then be represented by a formula.

Figure 2.2 shows graphical representations of some typical longitudinal friction characteristics. The initial rate at which  $\mu(s)$  increases with increasing slip is dependent on the properties of the tire. For wet and dry asphalt the characteristics increase until a peak value  $\mu_p = \mu(s_p)$  is attained. This typically occurs between 10 and 20 percent slip, yielding maximum braking forces of 25-50 and 70-90 percent of the vertical load for wet and dry asphalt, respectively. The friction characteristics then exhibit a gradual decrease to  $s = 1$  (wheel lockup). For gravel and packed snow, the behavior of the friction coefficient characteristics are qualitatively different. Peak values occur at wheel lockup (here,  $s = s_p = 1$ ) and are the consequence of plowing conditions on the deformable surfaces. Ice characteristics (not shown) are similar to those for wet and dry asphalt, differing mostly in the resulting peak values [1, 2, 3].

An analytical treatment of these friction characteristics is possible by employing the widely used Pacejka tire model [4, 5]. It is described by the so-called *Magic Formula* which is given by

$$y(x) = D \sin(C \arctan(Bx - E(Bx - \arctan(Bx)))), \quad (2.6)$$

where the parameters  $B$ ,  $C$ ,  $D$ , and  $E$  are the *stiffness*, *shape*, *peak*, and *curvature* factors. See reference 4 for typical values of these coefficients. Horizontal and vertical shifts of a characteristic are attained by the transformations

$$Y(\chi) = y(x) + S_v, \quad x = \chi + S_h,$$

where  $S_v$  is the vertical shift and  $S_h$  is the horizontal shift. The function  $Y(\chi)$  can

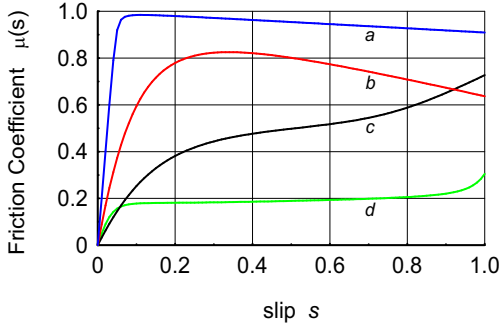


Figure 2.2. Typical longitudinal friction characteristics: (a) dry asphalt; (b) wet asphalt; (c) gravel; and (d) packed snow.

represent all steady-state tire characteristics—including the brake force  $X$ , side force, and self-aligning torque—in a physically meaningful and straightforward way. The variable  $\chi$  denotes either slip angle (the angle subtended from the direction of wheel travel to the direction of wheel heading) or longitudinal wheel slip  $s$ . In light of Equation (2.2) and Equation (2.5), note that the Magic Formula can be scaled to represent  $\mu(s)$  directly on  $I$ .

For the purpose of more efficient numerical simulations, a simple friction characteristic was devised for the present study and is given by

$$\mu(s) = c_1 (1 - e^{-c_2 s}) - c_3 s. \quad (2.7)$$

For  $c_1 = 1.18$ ,  $c_2 = 10.0$ , and  $c_3 = 0.5$ , this behaves similarly to wet and dry asphalt characteristics and has a peak value of  $\mu_p = 0.972$  at  $s_p = 0.316$ . This characteristic was employed for all calculations and numerical simulations involving  $\mu(s)$  in this chapter and in subsequent chapters.

## 2.2 Equations of Motion

During wheel slip, the single-wheel model possesses two dynamic states and hence requires a set of two coordinates to describe its motion. By inspection of Equations (2.1-2.5), it is clear that two of three possible variables of interest could be chosen as the independent variables, namely,  $u$ ,  $\omega$ , or  $s$ . The equations of motion for the single-wheel braking model are developed first in terms of  $u$  and  $\omega$  as dynamic states, and the qualitative dynamics are captured in the  $(u, \omega R)$  phase plane. Though such a description is physically enlightening, it is subsequently shown in Section 2.2.3 that a formulation of the equations of motion in terms of  $u$  and  $s$  as dynamics states lends itself to a relatively simple interpretation. Specifically, it will be shown that the latter formulation allows the dynamics for the entire range of vehicle speeds and slip values to be captured by a single function that is defined in terms of wheel slip and the brake torque.

### 2.2.1 $u$ and $\omega$ as Dynamic States

One possible formulation of the equations of motion is to use the speed  $u$  of the vehicle relative to ground and the absolute rotational rate  $\omega$  of the tire/wheel as dynamic states. Then the system dynamic equations are

$$\left. \begin{aligned} \dot{u} &= -\mu(u, \omega)g \\ \dot{\omega}R &= gH(u, \omega) \end{aligned} \right\}, \quad 0 \leq \omega R \leq u \quad (2.8)$$

where wheel slip is merely an internal variable. The restriction  $0 \leq \omega R \leq u$  ensures that  $s \in I$ , according to the convention of wheel slip in braking. The function

$$H(u, \omega) = \Psi\mu(u, \omega) - \Upsilon_b \quad (2.9)$$

is dimensionless, where  $\Psi = \frac{mR^2}{J}$  is the dimensionless ratio of vehicle to wheel inertia, and  $\Upsilon_b = \frac{R}{Jg}T_b$  is the dimensionless brake torque.

### 2.2.2 The $(u, \omega R)$ Phase Plane

Figure 2.3 shows trajectories in the  $(u, \omega R)$  state space for  $\Psi = 15$  and various dimensionless brake torque values. The rolling speed  $\omega R$  of the tire is defined along the ordinate while the vehicle speed  $u$  is defined along the abscissa. Wheel slip is implicitly defined in terms of these states by

$$\omega R = (1 - s)u, \quad (2.10)$$

which follows from the definition given by Equation (2.4). Equation (2.10) shows that radial lines originating from  $(u, \omega R) = (0, 0)$  are lines of constant slip for which there is a linear relationship between  $u$  and  $\omega R$ . Since  $s$  is defined on the unit interval for vehicle braking, the dynamics need only be considered in the region

$$\mathcal{F} = \{(u, \omega R) \mid u \geq 0, 0 \leq \omega R \leq u\}. \quad (2.11)$$

Thus, trajectories are bounded by the line  $\omega R = u$ , which corresponds to  $s = 0$  (free rolling), and the line  $\omega R = 0$ , or the  $u$ -axis, which corresponds to  $s = 1$  (wheel lockup). For a particular brake torque, some constant-slip radial lines are invariant under the dynamics and evolve only when the brake torque varies. The corresponding constant slip values shall be denoted by  $s^*$ . Any such set that satisfies these conditions and the equations of motion define invariant linear manifolds in the  $(u, \omega R)$  phase plane, which are denoted by

$$\mathcal{W}_b^* = \{(u, \omega R) \mid \omega R = (1 - s^*)u, s^* \in I\}. \quad (2.12)$$

Under certain conditions (to be determined subsequently), the  $u$  axis is also an invariant manifold (where  $s = 1$ ) and is denoted by

$$\mathcal{W}_b^L = \{(u, \omega R) \mid u \geq 0, \omega R = 0\}. \quad (2.13)$$

As shown in Figure 2.3a, there is a single invariant manifold  $\mathcal{W}_b^*$  when  $\Upsilon_b = 7$ . At this parameter value, initial conditions started in  $\mathcal{F}$  yield stable braking conditions (as opposed to lockup conditions), since all trajectories—including those started on  $\mathcal{W}_b^L$ —rapidly approach  $\mathcal{W}_b^*$  for decreasing  $u$  and evolve essentially along the invariant manifold toward zero speed at  $(u, \omega R) = (0, 0)$ . As the brake torque is increased to  $\Upsilon_b = 12$  two additional invariant manifolds are introduced, one of which corresponds to lockup conditions, that is,  $\mathcal{W}_b^L$ . This is shown in Figure 2.3b. For very large brake torques, all trajectories started in  $\mathcal{F}$  yield lockup conditions. Figure 2.3d shows this situation when  $\Upsilon_b = 18$ .

The diagrams depicted in Figure 2.3 show that, for decreasing  $u$ , trajectories tend rapidly toward either  $\mathcal{W}_b^*$  or  $\mathcal{W}_b^L$ , depending on the brake torque level. Hence, the invariant manifolds, if they exist, serve two purposes: they (1) define steady-slip conditions that are invariant under the dynamics and under which the vehicle decelerates to zero speed and (2) separate regions of stable and unstable braking. It would be desirable to quantify these manifolds without having to perform numerical simulations.

In what follows, an alternative formulation is considered where wheel slip  $s$  replaces  $\omega R$  as a dynamic state. Figure 2.4 compares the state space description of the single-wheel braking model in the  $(u, \omega R)$  phase plane to its description in the  $(u, s)$  phase plane for  $\Psi = 15$  and  $\Upsilon_b = 12$ . The alternative formulation yields a state space where, essentially, the point  $(u, \omega R) = (0, 0)$  is expanded to represent wheel slip on the unit interval. In doing so, a singularity is introduced at  $u = 0$ ; but, as

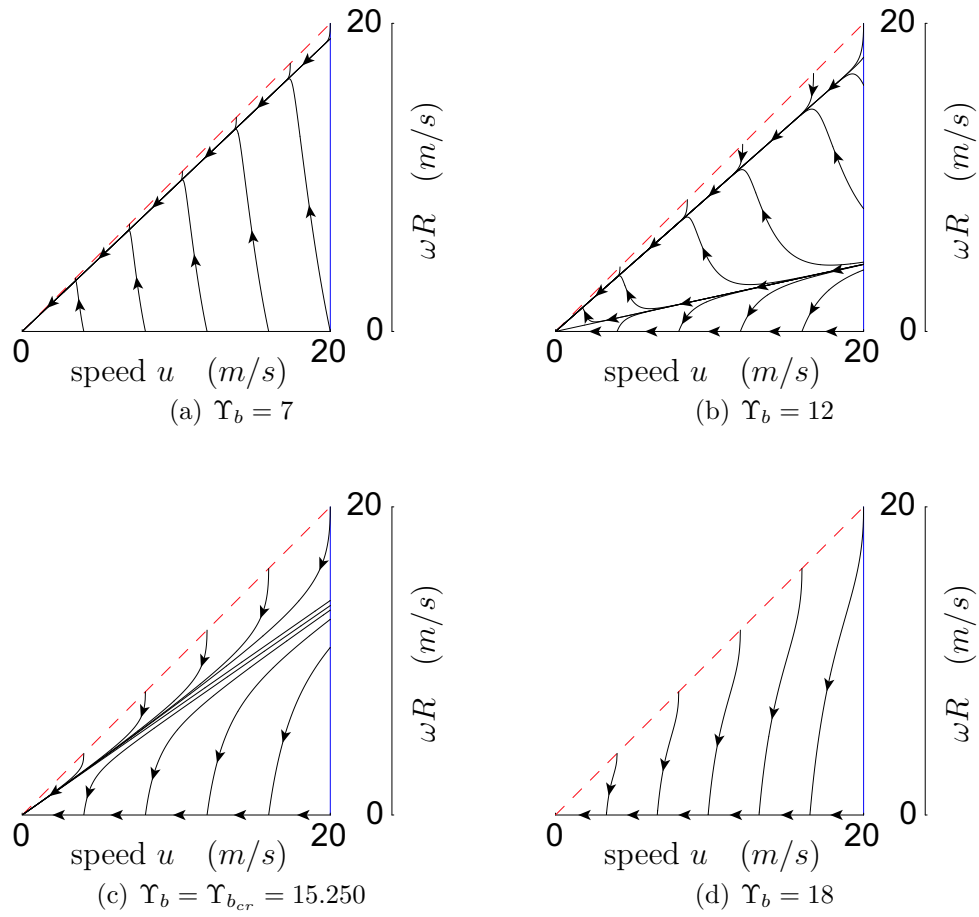


Figure 2.3. State space descriptions for the single-wheel braking model in the  $(u, \omega R)$  state space for  $\Psi = 15$ : (a)  $\Upsilon_b = 7$ ; (b)  $\Upsilon_b = 12$ ; (c)  $\Upsilon_b = \Upsilon_{b_{cr}} = 15.250$ ; (d)  $\Upsilon_b = 18$ .

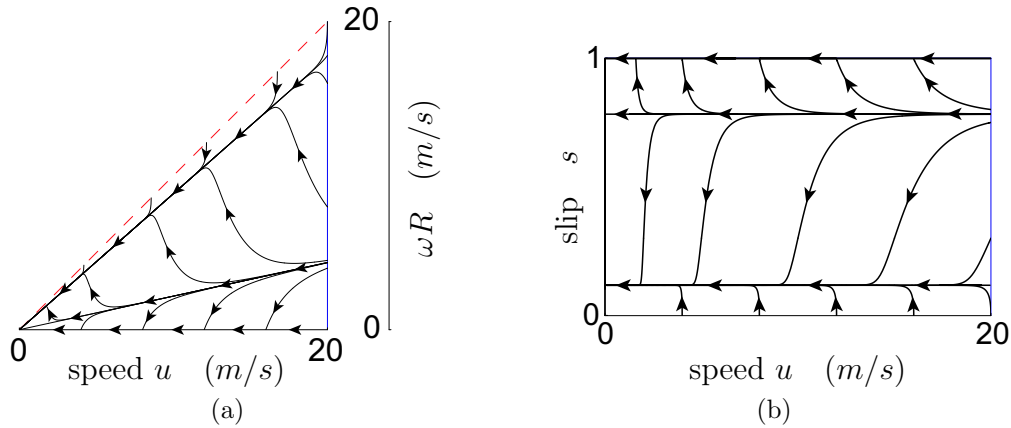


Figure 2.4. State space descriptions for the single-wheel braking model for  $\Psi = 15$  and  $\Upsilon_b = 12$ : (a) in  $u$  and  $\omega R$ ; (b) in  $u$  and  $s$ .

indicated in Figure 2.4b, the invariant manifolds  $\mathcal{W}_b^*$  and  $\mathcal{W}_b^L$  are easily identified in the  $(u, s)$  phase space as lines of constant  $s$ . It will be shown that a formulation of the equations of motion in terms of  $u$  and  $s$  allows for the invariant manifolds, and hence steady-slip conditions and various operating regimes, to be captured by a single function that is defined in terms of wheel slip and the brake torque.

### 2.2.3 $u$ and $s$ as Dynamic States

Although it is very natural to cast the equations of motion in terms of the forward vehicle speed  $u$  and the tire/wheel rate of rotation, it is instructive to replace  $\omega$  with wheel slip as a state variable. Liu and Sun [6] have developed the equations of motion for a quarter-car model using  $u$  and  $s$  as dynamic states, but their investigation focuses on control algorithms based on gain-scheduling. Here the equations of motion are developed similarly but with emphasis on a form suitable for a nonlinear dynamic

analysis. Evaluating the time rate of change of wheel slip (for  $\omega R \leq u$ )

$$\dot{s} = \frac{R}{u^2}(\omega\dot{u} - u\dot{\omega}),$$

and performing the appropriate substitutions, the equations of motion in terms of  $u$  and  $s$  can be cast in the form

$$\left. \begin{aligned} \dot{u} &= -\mu(s)g \\ \dot{s} &= \frac{g}{u}h_b(s) \end{aligned} \right\}, \quad u > 0, \quad s \in I. \quad (2.14)$$

Since  $u > 0$  by convention,  $g > 0$  and  $\mu(s) \in I$ , it follows that  $\dot{u} < 0$ , which is expected. The function

$$h_b(s) = (s - 1)\mu(s) - \Psi\mu(s) + \Upsilon_b, \quad (2.15)$$

is nondimensional, where, recall,  $\Psi = \frac{mR^2}{J}$  is the ratio of vehicle inertia to wheel inertia and  $\Upsilon_b = \frac{R}{Jg}T_b$  is the dimensionless brake torque.

The general features of the quarter-car model are best demonstrated by treating Equation (2.14) as a state-space representation of the single-wheel system and exploring their behavior in the  $(u, s)$  state space. It will be shown that this interpretation of the single-wheel model yields good insight into its dynamic response in transient and steady-state braking. The analysis begins by determining the steady-slip conditions and their local stability characteristics. A more detailed mathematical analysis follows in a discussion of the global features of the single-wheel braking model.

## 2.3 Steady-Slip Conditions

Equation (2.14) shows that, for nonzero  $u$  and a slip value  $s^*$  for which  $h_b(s^*) = 0$ , the time rate of change of slip is identically equal to zero. Correspondingly, wheel slip remains constant at  $s = s^*$ , independent of the vehicle speed. This in turn ensures that the vehicle acceleration  $\dot{u} = -\mu(s^*)g$  is negative and constant. Here,  $\mu(s^*)$  is the longitudinal force coefficient corresponding to the fixed slip value. Under these conditions the vehicle speed monotonically decreases to zero according to the equation

$$u(t) = u_o - \mu(s^*)gt, \quad u > 0, \quad t_f > t \geq 0, \quad (2.16)$$

where  $u_o > 0$  is the initial speed at the instant when  $s = s^*$ , that is, when  $t = 0$ .  $t_f$  corresponds to the time when  $u = 0$ . Wheel lockup also yields steady-slip conditions when  $s = 1$ . Under lockup conditions, the dynamics of the vehicle are described by Equation (2.16), with the coefficient of sliding friction  $\mu_L = \mu(s = 1)$  replacing  $\mu(s^*)$ .

## 2.4 Local Stability of Slip Dynamics

Before specifying a quantitative measure of stability, it is convenient to outline and adopt specific notation. First, recall that constant slip values  $s^*$  denote invariant points in the slip dynamics. They may be obtained by finding the zeros of  $h_b(s)$  or, equivalently, by finding the roots of  $h_b(s^*) = 0$ . More precisely, the steady-slip values  $s^*$ , if they exist, define *invariant sets* of the system, since once  $s = s^*$  is attained,  $s$  remains at that value for all time, independent of the values of  $u$  (for  $u > 0$ ). Any such value of  $s = s^*$  may be either stable or unstable and shall be denoted by  $s^+$  and  $s^-$ , respectively. Local stability criteria of wheel slip follows from considering a small perturbation  $\eta(t) = s(t) - s^*$  away from one of these roots. Differentiating with respect to time, invoking Equation (2.14), and employing  $h_b(s^*) = 0$ , the local slip

dynamics near  $s^*$  can be approximated to leading order by the linearized equation

$$\dot{\eta} = \frac{g}{u} h'_b(s^*) \eta, \quad (2.17)$$

where  $(\ )' = \frac{d}{ds}$  denotes differentiation with respect to  $s$ . Since  $\frac{g}{u} > 0$ , Equation (2.17) shows that the perturbation grows exponentially fast when  $h'_b(s^*) > 0$  and decays exponentially when  $h'_b(s^*) < 0$ . Thus, the stability of the slip dynamics near  $s = s^*$  are determined by the slope

$$h'_b(s^*) = \mu'(s^*) (s^* - 1 - \Psi) + \mu(s^*) \quad (2.18)$$

of  $h_b(s)$  at  $s = s^*$ . Stable and unstable steady-slip values are defined to be

$$s^\pm = \{s \mid h_b(s^\pm) = 0, h'_b(s^\pm) \leq 0\}. \quad (2.19)$$

The corresponding stable and unstable invariant manifolds of the system in the  $(u, s)$  plane are defined by

$$\mathcal{W}_b^\pm = \{(u, s) \mid u > 0, s = s^\pm\}. \quad (2.20)$$

Since wheel slip is restricted to the unit interval,

$$\mathcal{W}_b^L = \{(u, s) \mid u > 0, s = 1, h(1) > 0\}$$

is also an invariant manifold, where  $L$  denotes wheel lockup. The notation  $\mathcal{W}_b^*$  shall refer to either of the invariant manifolds  $\mathcal{W}_b^+$  or  $\mathcal{W}_b^-$ .

## 2.5 Global Features of the Single-Wheel Braking Model

Equation (2.17) and Equation (2.19) hint at the importance of the function  $h_b(s)$ , since steady-slip conditions and the local stability of the slip dynamics are completely determined in terms of this dimensionless function. In fact, the entire range of vehicle speeds and slip values are captured by  $h_b(s)$  under a constant brake torque or slowly varying brake torque. This is shown in Figure 2.5, where the function  $h_b(s)$  versus slip and the corresponding state space dynamics in  $u$  and  $s$  are depicted for  $\Psi = 15$  and for various values of the nondimensional brake torque. The intersection of the function  $h_b(s)$  with the line  $h_b = 0$  defines the invariant points  $s^*$  (see Equation 2.19 and Table 2.1), and hence the invariant manifolds  $\mathcal{W}_b^*$  in the  $(u, s)$  space, which are defined by Equation (2.20).

For  $\Upsilon_b = 7$ , a small brake torque, only one invariant point exists, which is shown in Figure 2.5a as  $s^+$ . Since  $h'_b(s^*) < 0$  the steady-slip value  $s^+$  is stable and hence defines the invariant manifold  $\mathcal{W}_b^+$ . All initial conditions  $(u, s) = \{(u, s) \mid u > 0, s \in I\}$  result in stable braking at this parameter value.

As the brake torque is increased to  $\Upsilon_b = 12$ , another fixed point has been introduced for which the slope of  $h'_b(s^*)$  is negative; hence it is unstable. It is denoted by  $s = s^-$  and defines the unstable invariant manifold  $\mathcal{W}_b^-$  in the  $(u, s)$  space. As shown in Figure 2.5b, all trajectories above  $\mathcal{W}_b^-$ , that is, those with initial conditions in  $\{(u, s) \mid u > 0, s \in (s^-, 1]\}$ , tend to  $\mathcal{W}_b^L$  (indicating wheel lockup). Trajectories lying below  $\mathcal{W}_b^-$  are attracted to the invariant manifold  $\mathcal{W}_b^+$  and result in stable braking conditions. Note that the creation of the unstable invariant point  $s^-$  corresponds to the introduction of stable lockup at  $s = 1$ . This is essentially a saddle-node bifurcation creating  $s^-$  and  $s = 1$  steady-slip values.

Further increasing  $\Upsilon_b$  causes  $s^+$  and  $s^-$  to move toward each other. Eventually a

critical brake torque  $\Upsilon_{b_{cr}} = 15.250$  is reached where the stable and unstable invariant points collide and mutually annihilate in a saddle node bifurcation at the critical slip value  $s = s_{cr} = 0.304$  (See Figure 2.5c.) For brake torques greater than  $\Upsilon_{b_{cr}}$  no stable points exist and wheel lockup occurs for all initial slip conditions. This situation is shown in Figure 2.5d where  $\Upsilon_b = 18$ .

Table 2.1. Steady-slip values for the single-wheel braking model

$\Upsilon_b$	$s^-$	$s_{cr}$	$s^+$
7	–	–	0.050
12	0.782	–	0.117
15.250	–	0.304	–
18	–	–	–

The set of initial conditions for which a trajectory reaches the stable invariant manifold  $\mathcal{W}_b^+$  is called the *domain of attraction* of  $s^+$  in the  $(u, s)$  state space and is denoted by  $\mathcal{D}$ . Clearly  $\mathcal{D}$  doesn't exist for post-bifurcation dynamics, since all initial conditions with  $u > 0$  would yield lockup conditions. For pre-bifurcation dynamics, that is, for  $\Upsilon_b < \Upsilon_{b_{cr}}$ ,

$$\mathcal{D} = \{(u, s) \mid u > 0, s \in I \setminus [s^-, 1]\}.$$

Trajectories started with initial conditions in  $\mathcal{D}$  rapidly converge toward the stable invariant manifold and evolve essentially along  $\mathcal{W}_b^+$ , according to Equation (2.16) toward the point  $(u, s) = (0, s^+)$ , where the vehicle stops. The rate at which the vehicle decelerates under steady-slip depends only on  $\mu(s^*)$ , that is, the particular friction characteristic and the value of  $s^*$ . All trajectories started outside  $\mathcal{D}$  and not on  $\mathcal{W}_b^-$  tend rapidly toward lockup at  $s = 1$ , subsequently move along  $\mathcal{W}_b^L$ ,

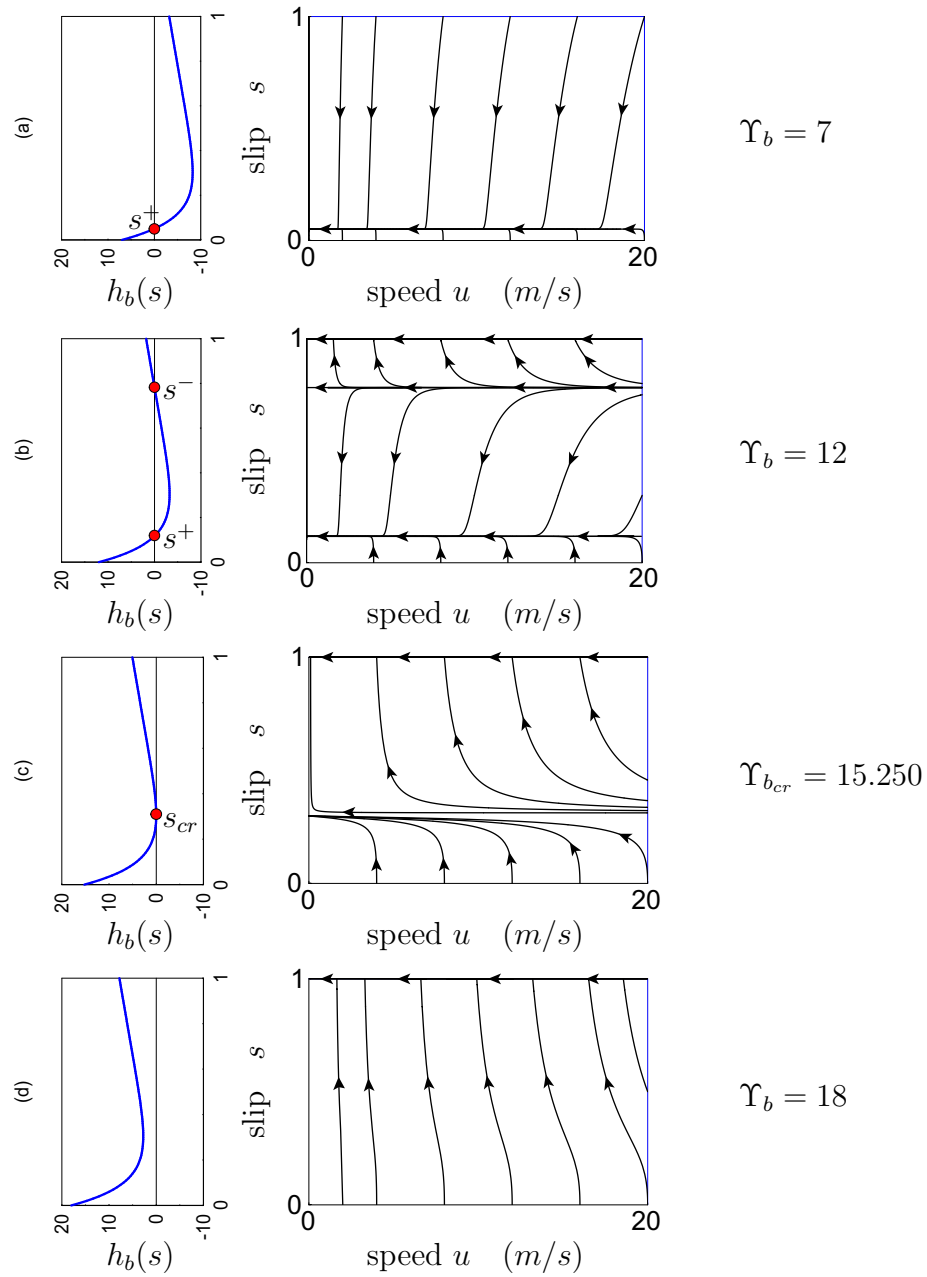


Figure 2.5.  $h_b(s)$  vs.  $s$  and corresponding state space descriptions in  $u$  and  $s$  for  $\Psi = 15$ : (a)  $\Upsilon_b = 7$ ; (b)  $\Upsilon_b = 12$ ; (c)  $\Upsilon_b = \Upsilon_{b_{cr}} = 15.250$ ; (d)  $\Upsilon_b = 18$ . See Table 2.1 for steady slip values.

and monotonically approach the point  $(0, 1)$ . This situation corresponds to braking under lockup conditions which, for wet and dry asphalt characteristics, is always non-optimum since  $\mu(s = 1) = \mu_L < \mu(s_p)$ . Finally, trajectories started on the unstable invariant manifold remain on  $\mathcal{W}_b^-$  and monotonically evolve toward the point  $(0, s^-)$ . This situation is physically impossible, however, since any small perturbation in the system would cause a trajectory to leave  $\mathcal{W}_b^-$  and tend rapidly toward either lockup or the stable invariant manifold.

Note that the rate at which a trajectory tends toward either  $\mathcal{W}_b^L$  or  $\mathcal{W}_b^+$  increases dramatically as  $u$  tends toward zero since  $\dot{s} \sim \frac{1}{u}$ . In fact, from Equation (2.14), the time rate of change of wheel slip becomes infinite as  $u \rightarrow 0$  with  $s \neq 1, s^*$ . Hence, the vehicle must come to rest *under steady-slip conditions* for which  $s = 1$  or  $s = s^*$ . There are only two such physical possibilities: the vehicle decelerates to zero speed (1) at the rate  $\mu_L g$  with the wheels locked or (2) with steady-slip at the absolute rate  $\mu(s^+)g$  (typically). Peak steady-braking performance would entail steady slip at  $s = s_p$  for which the maximum deceleration is equal in magnitude to  $\mu_p g$ . However, a steady-slip value  $s^* = s_p$  is always unstable. Thus, since  $s_p$  cannot be reached under stable braking conditions, optimum braking would entail steady-slip at  $s = s_{cr}$ . The corresponding deceleration is equal in magnitude to  $\mu_{cr} g = \mu(s = s_{cr})g < \mu_p g$ . But since  $s_{cr}$  is a saddle node in the slip dynamics, any perturbation in the system could send the braking conditions into wheel lockup. The critical brake torque needed to sustain optimum braking, and the corresponding lockup instability at that brake torque value, are discussed in Section 2.7.

It is again stressed that the function  $h_b(s)$  completely determines the nonlinear dynamic behavior of the single-wheel system in braking over the entire range of vehicle speeds and slip values. Given the dimensionless brake torque  $\Upsilon_b$ , one needs only calculate the zeros of  $h_b(s)$  to quantify steady-slip values and the corresponding invariant sets. The slope of  $h_b(s)$  at these steady-slip values indicates the stability

of the corresponding invariant manifolds. With this knowledge, a complete phase plane description of the vehicle dynamics can be constructed for the brake torque of interest from which information on regions of stable and unstable braking can be easily extracted.

## 2.6 Hysteresis in the Single-Wheel Braking Model

The dimensionless function  $h_b(s)$  and the  $(u, s)$  dynamics reveal certain features of the system that may otherwise be difficult to extract. Referring again to Figure 2.5, consider the case when the saddle-node bifurcation has already occurred and that the current state of the system is that of wheel lockup (Figure 2.5d). One may intuitively guess that the brake torque need only be reduced to a value slightly less than  $\Upsilon_{b_{cr}} = 15.250$  in order for stable braking to again be restored. This, however, is not the case. Although the stable invariant point  $s^+$  reappears, the state of the system remains at  $(u, 1)$ , or wheel lockup since that point remains stable as well. In fact,  $\Upsilon_b$  must be more drastically reduced to a value such that  $h_b(1) < 0$ , that is, lockup must be destabilized, in order to restore stable braking conditions. Once this occurs, the system state jumps from wheel lockup to stable braking conditions.

## 2.7 The Transition to Unstable Braking

When a brake torque is applied to a rubber tire a tractive force is generated at the tire/road interface, as described in Section 2.1. The standard thinking is that the brake torque can increase until wheel slip reaches the value  $s_p$ , beyond which lockup occurs [1, 2]. Under steady-state braking conditions, the corresponding maximum

brake torque is typically assumed to be

$$T_{b_p} = mgR\mu(s_p), \quad (2.21)$$

which is the peak moment provided by the friction force  $X = \mu(s_p)Z = \mu(s_p)mg$  about the wheel center. Thus, it is traditionally assumed that the critical brake torque for which the lockup instability is impending and the peak brake torque are the same, and that the transition to wheel lockup occurs at  $s = s_p = s_{cr}$ . In what follows, it is shown that the lockup instability does not occur at the peak value  $s_p$  corresponding to the maximum of the  $\mu(s)$  curve, but at a condition that is typically nearby. It is subsequently shown that Equation (2.21) is actually only an approximation that is accurate when the inertia ratio  $\Psi$  is large.

### 2.7.1 Lockup Instability

For the single-wheel braking model the function  $h_b(s)$  can be written in the form

$$h_b(s) = \mu(s)(s - 1 - \Psi) + \Upsilon_b. \quad (2.22)$$

Differentiating Equation (2.22) with respect to  $s$  and evaluating the resulting expression at critical slip yields

$$h'_b(s_{cr}) = \mu'(s_{cr})(s_{cr} - 1 - \Psi) + \mu(s_{cr}) = 0, \quad (2.23)$$

where, recall,  $s_{cr}$  is the saddle node value in the slip dynamics. Since in Equation (2.23),  $\mu(s_{cr}) > 0$  and  $(s_{cr} - 1 - \Psi) < 0$ , it follows that

$$\mu'(s_{cr}) = \frac{-\mu(s_{cr})}{s_{cr} - 1 - \Psi} > 0. \quad (2.24)$$

Equation (2.24) shows that the slope of the friction characteristic at the critical value  $s = s_{cr}$  is positive, rather than zero, which is the case at  $s_p$ . This means that, for wet or dry asphalt characteristics,  $s_{cr}$  is actually *smaller* than the peak value  $s_p$ . Hence, the lockup instability, or the transition to unstable braking, corresponds not to  $s_p$ , the peak of  $\mu(s)$ , but to the critical value  $s_{cr}$ , the minimum of  $h_b(s)$ . These results are consistent with numerical evidence. Recall that the peak value  $\mu_p = \mu(s = s_p)$  of Equation (2.7) occurs at  $s_p = 0.316$ , whereas  $s_{cr} = 0.304$ , which is approximately 4 percent less than  $s_p$ . The corresponding critical brake torque is outlined next, from which Equation (2.21) can be obtained by invoking a series of approximations.

### 2.7.2 The Critical Brake Torque

Recall from Section 2.5 that the vehicle must come to rest under steady-slip conditions for which  $s = 1$  (wheel lockup) or  $s = s^*$ . The brake torque corresponding to a steady-slip value  $s = s^*$  follows from Equation (2.22) and is given by

$$\Upsilon_b = -\mu(s^*)(s^* - 1 - \Psi), \quad (2.25)$$

where the condition  $h_b(s^*) = 0$  has been invoked. The maximum possible brake torque corresponding to steady-slip conditions is obtained by maximizing Equation (2.25).

The result is

$$\left. \frac{\partial \Upsilon_b}{\partial s} \right|_{s=s^*} = \mu'(s^*)(s^* - 1 - \Psi) + \mu(s^*) = 0. \quad (2.26)$$

Equation (2.26) is of the same form as Equation (2.23), which is an expression that minimizes  $h_b(s)$ . Thus, it must be true that the maximum brake torque is given by Equation (2.22) with the steady-slip value  $s^* = s_{cr}$  satisfying Equation (2.23). Recalling that  $\Upsilon_b = \frac{R}{Jg}T_b$  and  $\Psi = \frac{mR^2}{J}$ , the critical brake torque can be written in

the dimensional form

$$T_{b_{cr}} = mgR\mu(s_{cr}) \left( 1 + \frac{1}{\Psi}(1 - s_{cr}) \right). \quad (2.27)$$

Equation (2.27) indicates that the typically assumed maximum brake torque given by Equation (2.21) follows from two fundamental assumptions: (1) the inertia ratio  $\Psi$  of the vehicle is large relative to unity, and (2) the peak slip value  $s_p$  can be attained. These assumptions are generally acceptable so that, for many applications, the true critical brake torque can be reasonably approximated by the assumed brake torque given by Equation (2.21). This is shown next.

Idealizing the wheel as a thin uniform disk of mass  $m_{wheel}$ , it follows that

$$\Psi = \frac{mR^2}{J} = 2\frac{m}{m_{wheel}}, \quad (2.28)$$

where, recall,  $m$  is the mass of the vehicle/wheel combination. In most applications  $m \gg m_{wheel}$  so that  $\Psi \gg 1$ . Moreover, the peak value  $s_p$  and  $s_{cr}$  are typically close. Referring again to Equation (2.7) and noting that  $\mu(s_{cr}) = \mu(0.304) = 0.972$ , it follows that  $\Upsilon_{b_p} = 14.574$  for  $\Psi = 15$ . Numerical simulations show that  $\Upsilon_{b_p} = 15.250$  (see Figure 2.5), rendering the approximation given by Equation (2.21) in error by less than five percent.

## 2.8 The Effects of Aerodynamic Drag and Rolling Resistance

The force  $X$  is the main source of vehicle deceleration during braking. However, there are other factors that may be of comparable importance. For high-speed braking, aerodynamic drag is the primary retarding force on a vehicle, whereas for very-low

speed braking, the primary retarding force is rolling resistance [1]. These factors are included in the single-wheel braking model here to show their effects on the system dynamic equations of motion.

A simple and commonly used model for aerodynamic drag on a vehicle is given by

$$F_D = \frac{1}{2}\rho AC_D u^2, \quad (2.29)$$

where  $\rho$  is the ambient air density,  $A$  is the projected frontal area of the vehicle, and  $C_D$  is an experimentally determined aerodynamic drag coefficient.

Rolling resistance depends on a number of interdependent factors including vehicle speed, wheel slip, and the tire temperature, pressure, loading, and construction. The total force acting on a vehicle due to the rolling resistance of each wheel is typically given in terms of the vehicle weight  $mg$  as

$$F_r = mgf_r, \quad (2.30)$$

where  $f_r$  is a rolling resistance coefficient. Several equations are available for estimating  $f_r$ , but their accuracy is limited since it is virtually impossible to account for all of the important physical properties of the tire and ground. If only a crude estimate of rolling resistance is desired,  $f_r$  may be taken to be constant. More accurate models for rolling resistance may be obtained, for example, by taking  $f_r$  to be speed dependent. Gillespie [1] cites some typically used empirical relationships for  $f_r(u)$ .

Including aerodynamic drag and speed dependent rolling resistance in the single-wheel braking model, the dynamic equations of motion take the form

$$\left. \begin{aligned} \dot{u} &= -\mu(s)g - F(u)g \\ \dot{s} &= \frac{g}{u}h_b(s) + \frac{g}{u}(s-1)F(u) \end{aligned} \right\}, \quad u > 0, \quad s \in I, \quad (2.31)$$

where  $h_b(s)$  is given by Equation (2.15). The function

$$F(u) = f_r(u) + \frac{\rho C_D A}{2mg} u^2 \quad (2.32)$$

is dimensionless and represents the effects of rolling resistance and aerodynamic loading on the vehicle dynamics. The  $u^2$  terms in Equation (2.32) indicate that aerodynamic drag becomes significant at higher vehicle speeds. Rolling resistance increases approximately linearly for low vehicle speeds and more closely obeys a speed-squared relationship for higher speeds [1]. Hence, its effects on the vehicle dynamics are important at all speeds, particularly at high speeds. The new function  $F(u)$  in Equation (2.31) renders the nonlinear dynamic analysis of the single-wheel model more complicated, since steady-slip values—and hence the system invariant manifolds—cannot be obtained simply by finding the roots of  $h_b(s) = 0$ . Invariant manifolds of the form  $u = \mathcal{G}(s)$  will exist, and can be determined by standard techniques [11]. These will describe the dynamics of  $(u, s)$  as the vehicle decelerates.

It should be noted that the primary advantage of using slip as a dynamic state is not realized in this model.

# CHAPTER 3

## The Single-Wheel Acceleration

### Model

This chapter describes a single-wheel vehicle acceleration model. Here, the term acceleration refers to the positive rate of change of velocity in the longitudinal direction due to an engine torque. Longitudinal acceleration is fundamentally dependent on two main limitations: engine power and traction [1]. However, the ensuing investigation assumes that sufficient engine power is available at any given instant to maintain a constant torque on the wheel. Thus, focus is shifted entirely to understanding tractive properties and their dynamic characteristics and how to maximize them.

The single-wheel vehicle acceleration model is physically identical to that of the single-wheel braking model, consisting of a wheel/tire disk with radius  $R$  and polar moment of inertia  $J$ . As depicted in Figure 3.1, it is constrained to move longitudinally in the  $x$ -direction with its speed denoted as  $u$ . The available engine torque, acting in the positive sense on the wheel, is denoted by  $T_e$ . The vertical reaction force  $Z$  balances the static weight  $mg$ , while the longitudinal force  $X$  serves to accelerate the vehicle.

As with the single-wheel braking model, the forward vehicle speed  $u$  and longitudinal wheel slip  $s$  are chosen as dynamic states. In vehicle acceleration it is

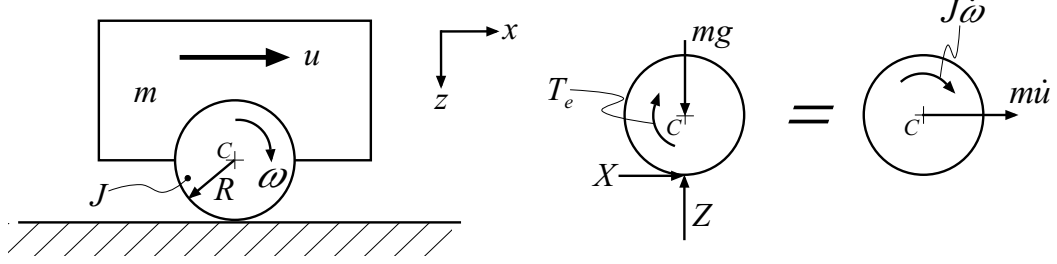


Figure 3.1. Schematic of the single-wheel acceleration model and corresponding free body diagram

assumed and taken as convention that  $\omega R > 0$  and  $0 \leq u \leq \omega R$ . Thus, wheel slip  $s = \frac{u - \omega R}{\max(u, \omega R)} = \frac{u - \omega R}{\omega R}$  is defined on the interval  $-I = [-1, 0]$ , taking on the limiting values  $s = -1$  for pure slip ( $u = 0$ ) and  $s = 0$  for free rolling without slip ( $u = \omega R > 0$ ). The former case when  $u = 0$  indicates finite rotation of the wheel while maintaining zero vehicle speed, which is shown in Section 3.2 to be an unstable condition. The case when  $u = \omega R$  implies the absence of an engine torque.

The Pacejka tire model can be employed in vehicle acceleration studies by letting  $s \rightarrow -s$  in the Magic Formula (Equation [2.6]). Similar to Equation (2.7), the characteristic

$$\mu(s) = c_1 (1 - e^{c_2 s}) + c_3 s \quad (3.1)$$

was used (with  $c_1 = 1.18$ ,  $c_2 = 10.0$ , and  $c_3 = 0.5$ ) in all numerical simulations in this paper involving vehicle acceleration models. It has a peak value  $\mu_p = 0.972$  at  $s = -s_p = -0.316$ .

### 3.1 Equations of Motion

Assuming that the friction law given by Equation (2.5) holds and making the appropriate substitutions, the equations of motion for the single-wheel acceleration model

can be cast in the form

$$\left. \begin{aligned} \dot{u} &= \mu(s)g \\ \dot{s} &= \frac{g}{u}h_t(s) \end{aligned} \right\}, \quad u > 0, \quad s \in (-1, 0]. \quad (3.2)$$

The nondimensional function  $h_t(s)$  is given by

$$h_t(s) = (s + 1)^2 [(s + 1)^{-1}\mu(s) + \Psi\mu(s) - \Upsilon_e], \quad (3.3)$$

where, again,  $\Psi = \frac{mR^2}{J}$  is the vehicle/wheel inertia ratio and  $\Upsilon_e = \frac{R}{Jg}T_e$  is the dimensionless engine torque.

## 3.2 Steady-Slip Conditions and Local Stability

For nonzero  $u$  and a constant slip value  $s^*$  for which  $h_t(s^*) = 0$ , Equation (3.2) shows that wheel slip remains invariant, independent of the vehicle speed. Correspondingly, the forward vehicle acceleration is positive and constant, and its speed monotonically increases according to the equation

$$u(t) = u_o + \mu(s^*)gt, \quad t \geq 0, \quad (3.4)$$

where  $u_o > 0$  is the initial speed when  $s = s^*$ , that is, when  $t = 0$ . Clearly the vehicle cannot continue to accelerate indefinitely. Due to aerodynamic drag, saturation of engine power, etc., generation of the prescribed engine torque eventually becomes impossible. In order to quantify this limiting case one must include other factors in the dynamic model, which will not be considered here.

Local stability of the invariant points  $s^*$  follows in the same way as discussed for the single-wheel braking model. (See Section 2.4.) Stable and unstable fixed points

are defined to be

$$s^\pm = \{s \mid h_t(s^\pm) = 0, h'_t(s^\pm) \leq 0\},$$

and the corresponding invariant manifolds are given by

$$\mathcal{W}_t^\pm = \{(u, s) \mid u > 0, s = s^\pm\}.$$

Note that the set  $\{(u, s) \mid u > 0, s = -1\}$  does not define an invariant manifold, since  $\dot{s}$  is singular when  $u = 0$ .

### 3.3 Global Features of the Single-Wheel Vehicle Acceleration Model

The dynamic equations describing the single-wheel acceleration model are of the same structure as their braking model counterparts, with the only significant differences appearing in  $h_t(s)$ . Whereas the brake torque appears simply as an additive term in the function  $h_b(s)$  of the single-wheel braking model (Equation [2.15]), the engine torque is scaled by the nonlinear term  $(s+1)^2$  in the function  $h_t(s)$  of the single-wheel acceleration model (Equation [3.3]). It is this nonlinearity that yields slightly more complicated dynamics as the parameter  $\Upsilon_e$  is varied.

Depicted in Figure 3.2 is the function  $h_t(s)$  versus slip and the corresponding state space dynamics in  $u$  and  $s$  for  $\Psi = 15$  and various values of the nondimensional engine torque. For  $\Upsilon_e = 7.5$  there exists a stable invariant point  $s^+$ , which defines an invariant manifold  $\mathcal{W}_t^+$ . All initial conditions  $\{(u, s) \mid u \geq 0, s \in [0, 1)\}$  result in stable acceleration at this parameter value, with trajectories tending toward  $\mathcal{W}_t^+$  at a rate which decreases with increasing speed. As they approach the stable manifold, trajectories evolve essentially along  $\mathcal{W}_t^+$ , and the vehicle accelerates according to

Table 3.1. Steady slip values for the single wheel acceleration model.

$\Upsilon_e$	$s^-$	$s_{cr}$	$s^+$
7.5	–	–	-0.054
15	–	–	-0.203
22.5	–	–	-0.940
14.65	–	–	-0.186
15.196	–	-0.695	-0.214
15.65	-0.507	–	-0.250
	–	–	-0.806
16.032	–	-0.350	-0.834
16.65	–	–	-0.862

Equation (3.4).

Further increasing the engine torque to  $\Upsilon_e = 15.0$  renders  $s^+$  slightly more negative and brings the relative maxima and minima of  $h_t(s)$  very close to the line  $h_t = 0$ . At this parameter value the vehicle experiences near-maximum acceleration. The nearly flat character of  $h_t(s)$  over a range of  $s$  in this torque range implies high sensitivity and rapid changes for small torque variations. An increase of the engine torque to  $\Upsilon_e = 22.5$  moves  $\mathcal{W}_t^+$  nearly to pure-slip conditions.

To investigate more closely the dynamic subtleties involved in the small engine torque range near maximum acceleration, consider Figure 3.3 and Figure 3.4. These figures show the function  $h_t(s)$  versus slip, and the corresponding state space descriptions in  $u$  and  $s$ , in detail near a rapid set of bifurcations over the torque range  $14.65 \leq \Upsilon_e \leq 16.65$ . The vehicle acceleration dynamics are rich over this torque range primarily due to the nonlinear term  $(s + 1)^2$  in the function  $h_t(s)$  (Equation [3.3]). Optimum steady acceleration conditions would entail steady-slip at  $s_p = -0.316$  (see Equation [3.1]) for which the maximum acceleration is equal to  $\mu(s_p)g$ . This condition occurs for engine torques near  $\Upsilon_e = 16$  (Figures 3.3c and 3.3d), though only a small set of initial conditions would yield *stable* acceleration at near optimum conditions.

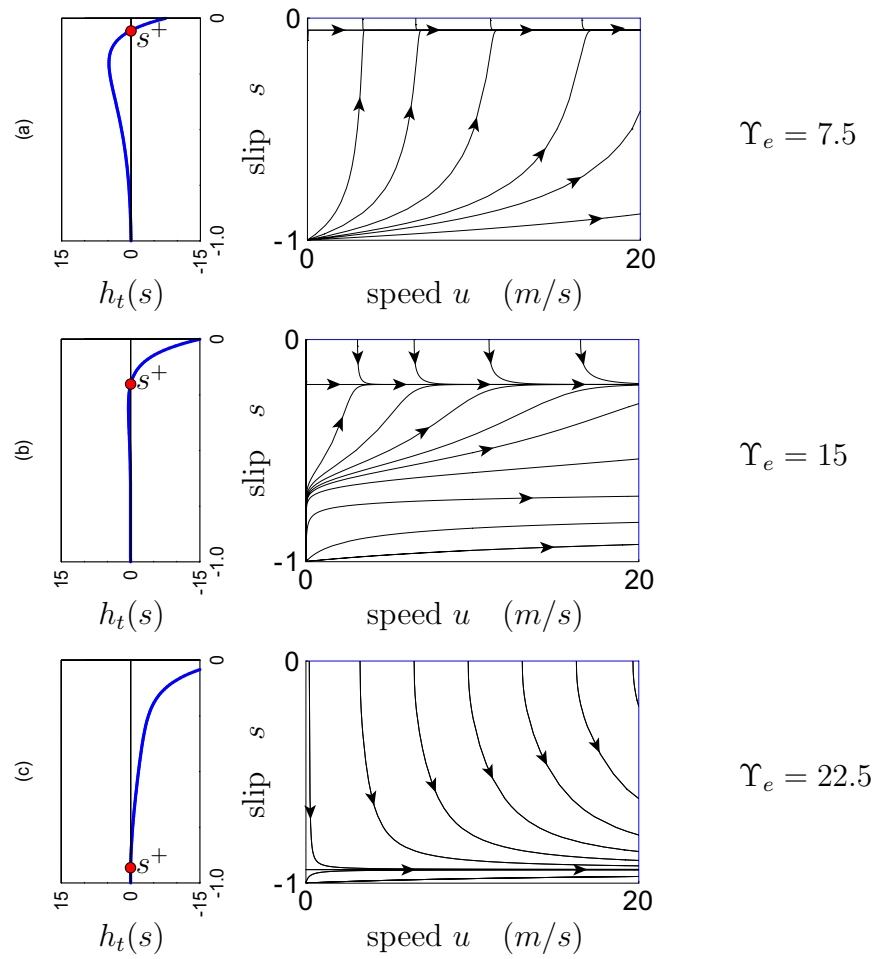


Figure 3.2.  $h_t(s)$  vs.  $s$  and corresponding state space descriptions in  $u$  and  $s$  for  $\Psi = 15$ : (a)  $\Upsilon_e = 7.5$ ; (b)  $\Upsilon_e = 15.0$ ; (c)  $\Upsilon_e = 22.5$ . See Table 3.1 for steady-slip values.

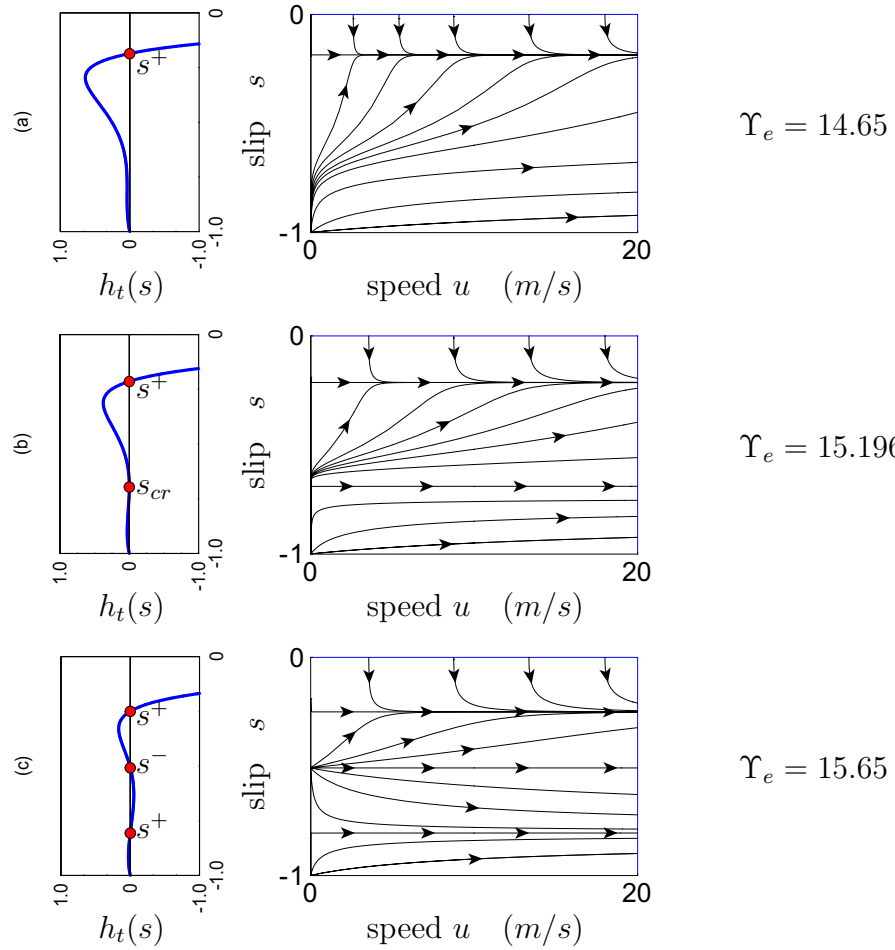


Figure 3.3.  $h_t(s)$  vs.  $s$  and corresponding state space descriptions in  $u$  and  $s$  in detail near a rapid set of bifurcations: (a)  $\Upsilon_e = 14.65$ ; (b)  $\Upsilon_e = 15.196$ ; (c)  $\Upsilon_e = 15.65$ . See Table 3.1 for steady-slip values.

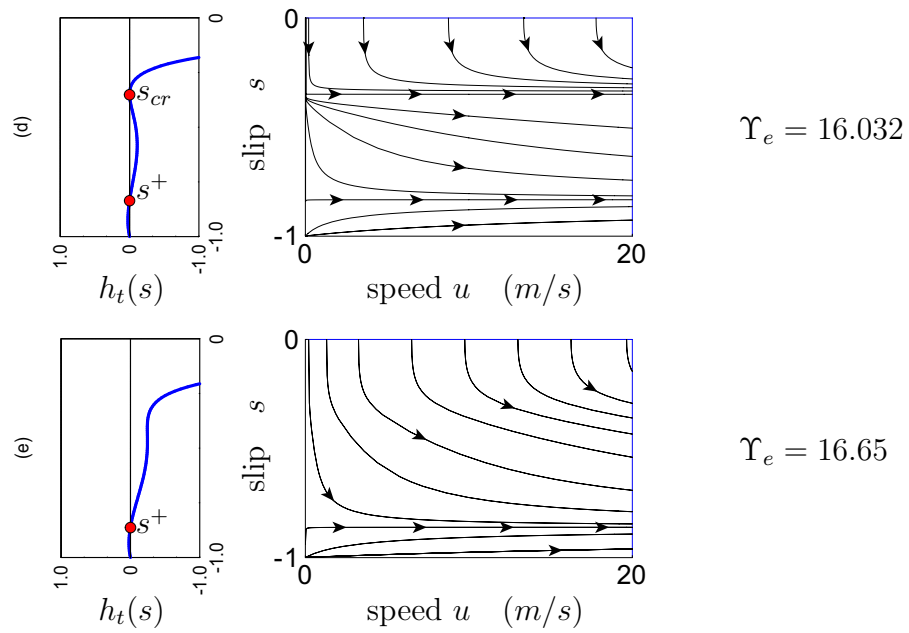


Figure 3.4.  $h_t(s)$  vs.  $s$  and corresponding state space descriptions in  $u$  and  $s$  in detail near a rapid set of bifurcations: (d)  $\Upsilon_e = 16.032$ ; (e)  $\Upsilon_e = 16.65$ . See Table 3.1 for steady-slip values.

# CHAPTER 4

## Two-Wheel Braking and Acceleration Models

### 4.1 The Two-Wheel Braking Model

A two-wheel vehicle braking model is developed in this chapter and is shown schematically in Figure 4.1. The entire weight  $mg$  of the vehicle is assumed to be concentrated at its mass center, which is located a length  $c$  forward of the rear axle and a distance  $h$  normal to the road surface. The front and rear wheels are assumed to be identical, each with an effective rolling radius  $R$  and polar moment of inertia  $J$ . Their centers are separated by a distance  $l = b + c$ . The vehicle moves longitudinally in the  $x$ -direction at a rate  $u$  along the road surface, which is inclined at an angle  $\theta$  below the horizontal.

The equations of motion describing the two-wheel vehicle braking model are developed in much the same way as in the single-wheel counterpart of Chapter 2. Where appropriate, a distinction is made between the rear and front wheels. Hence, each wheel requires its own description of longitudinal and reaction forces, slip, and circumferential speed. To this end, the rear and front longitudinal forces are defined

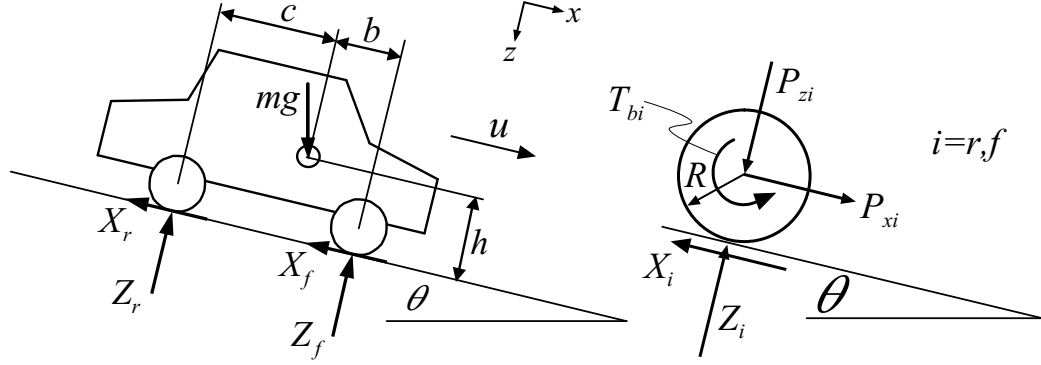


Figure 4.1. Schematic of the two-wheel braking model and corresponding free body diagram of a single wheel

using Equation (2.4) and are given by\*

$$X_i = \mu(s_i)Z_i, \quad i = r, f. \quad (4.1)$$

Similarly, rear and front slip are defined using Equation (2.4) as

$$s_i \equiv \frac{u - \omega_i R}{\max(u, \omega_i R)}, \quad i = r, f. \quad (4.2)$$

It is taken as convention that  $u > 0$  and  $0 \leq \omega_i R \leq u$  ( $i = r, f$ ) for braking. Thus,  $s_i = \frac{u - \omega_i R}{u}$  ( $i = r, f$ ) are defined on the unit interval  $I$ , allowing for free rolling, finite slip, or lockup of the rear and/or front wheels. The introduction of another independently rolling wheel in the vehicle braking model renders the front and rear reaction forces as dynamic terms in the equations of motion, that is, they become acceleration dependent. This phenomenon is known as *dynamic load transfer* [1] and

---

\*The force coefficient  $\mu(s_i)$  can take different values, depending on the respective values of  $s_i$  ( $i = r, f$ ). Note, however, that the longitudinal force coefficient characteristic is of one type only (e.g., wet or dry asphalt), assuming that the tires are of the same type and condition.

is captured by the normal forces acting on the tires

$$Z_r = mg \left( \frac{b}{l} \cos \theta - \frac{h}{l} \sin \theta \right) + m\dot{u} \frac{h}{l}, \quad (4.3)$$

$$Z_f = mg \left( \frac{c}{l} \cos \theta + \frac{h}{l} \sin \theta \right) - m\dot{u} \frac{h}{l}. \quad (4.4)$$

The first terms on the right hand side of Equations (4.3) and (4.4) are recognized to be static loads  $(Z_r)_{stat}$  and  $(Z_f)_{stat}$  on the rear and front wheels. The term  $m\dot{u} \frac{h}{l}$  is defined as the *dynamic load transfer*. Since  $\dot{u} < 0$  this term is negative for vehicle braking. Thus, in agreement with intuition, dynamic load transfer has the effect of shifting normal loads from the rear wheel to the front wheel during braking.

### 4.1.1 Equations of Motion

During wheel slip, the two-wheel model possesses three dynamic states and hence requires a set of three coordinates to describe its motion. Similar to the single-wheel model analysis, the states  $u$ ,  $s_r$ , and  $s_f$  are chosen for the ensuing analysis. With the appropriate substitutions, the dynamics of the two-wheel system are governed by the equations

$$\left. \begin{aligned} \dot{u} &= -g (\Lambda_b(\mathbf{s}) \cos \theta - \sin \theta) \\ \dot{\mathbf{s}} &= \frac{g}{u} \mathbf{h}_b(\mathbf{s}) \end{aligned} \right\}, \quad u > 0, \quad \mathbf{s} \in I \times I. \quad (4.5)$$

where  $\mathbf{s} = (s_r, s_f)$  and  $\mathbf{h}_b(\mathbf{s}) = (h_{br}(\mathbf{s}), h_{bf}(\mathbf{s}))$  are vectors, and  $g$  is the acceleration due to gravity. The function

$$\Lambda_b(\mathbf{s}) = \frac{\mu(s_r) \frac{b}{l} + \mu(s_f) \frac{c}{l}}{1 + \frac{h}{l} (\mu(s_r) - \mu(s_f))}$$

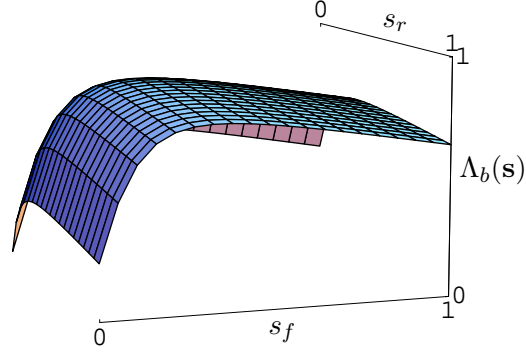


Figure 4.2.  $\Lambda_b(\mathbf{s})$  for  $h = 1.25$ ,  $c = 6$ ,  $b = 4$ , and  $\theta = 0$ . A wet asphalt friction characteristic has been employed.

is a measure of the nondimensional vehicle deceleration in the direction of the vehicle heading. An example plot of  $\Lambda_b(\mathbf{s})$  is shown in Figure 4.2. The scalar functions

$$h_{bi}(\mathbf{s}) = (s_i - 1) (\Lambda_b(\mathbf{s}) \cos \theta - \sin \theta) - \mu(s_i) \Psi \lambda_i(\mathbf{s}) + \Upsilon_{bi}, \quad i = r, f \quad (4.6)$$

are dimensionless, where  $\Psi = \frac{mR^2}{J}$  is the vehicle/wheel inertia ratio (as before), and  $\Upsilon_{bi} = \frac{R}{Jg} T_{bi}$  ( $i = r, f$ ) are the rear and front dimensionless brake torques, and the parameters

$$\left. \begin{aligned} \lambda_r(\mathbf{s}) &= \left( \frac{b}{l} - \Lambda_b(\mathbf{s}) \frac{h}{l} \right) \cos \theta \\ \lambda_f(\mathbf{s}) &= \left( \frac{c}{l} + \Lambda_b(\mathbf{s}) \frac{h}{l} \right) \cos \theta \end{aligned} \right\} \quad (4.7)$$

are the nondimensional dynamic normal loads on the rear and front wheels, respectively. Example plots of  $h_{br}(\mathbf{s})$  and  $h_{bf}(\mathbf{s})$  are shown in Figure 4.3.

### 4.1.2 Steady-Slip Conditions

The relationship between slip values  $s_r$  and  $s_f$  and the forward vehicle speed becomes clear by invoking a Leibniz notation scheme, forming a ratio of  $\dot{s}_r$  and  $\dot{s}_f$ , and invoking

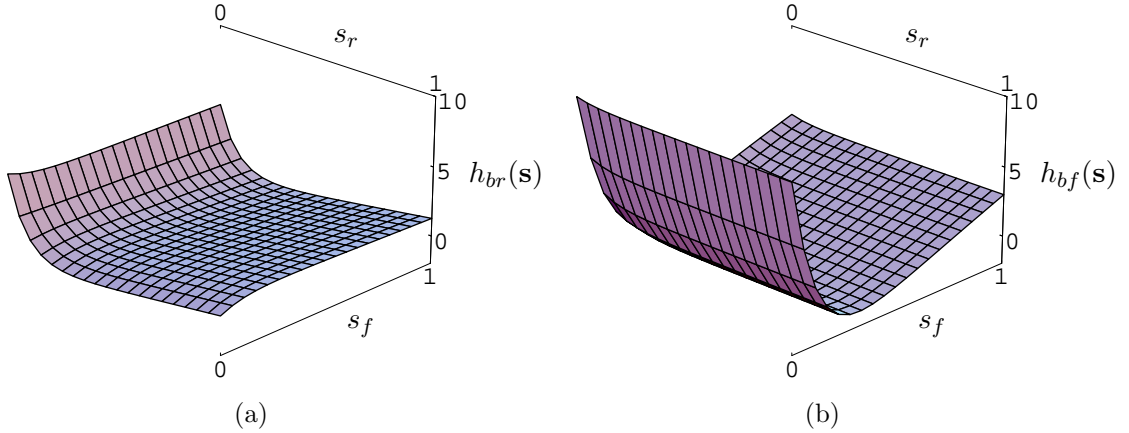


Figure 4.3. The functions (a)  $h_{br}(\mathbf{s})$  and (b)  $h_{bf}(\mathbf{s})$  for  $h = 1.25$ ,  $c = 6$ ,  $b = 4$ ,  $\theta = 0$ ,  $\Psi = 15$ ,  $\Upsilon_{br} = 3.5$ , and  $\Upsilon_{bf} = 10.0$ .

Equation (4.5). Then

$$\frac{ds_r}{ds_f} = \frac{h_r(\mathbf{s})}{h_f(\mathbf{s})}, \quad (4.8)$$

which shows that relative dynamic changes in  $s_r$  and  $s_f$  are a function of the ratio of  $h_{br}(\mathbf{s})$  to  $h_{bf}(\mathbf{s})$ , and are *independent* of  $u$ . That is, relative changes in rear and front slip are *invariant* to changes in the vehicle speed. Thus it suffices, for a qualitative description of the dynamics, to examine a state space in the independent variables  $s_r$  and  $s_f$ . Although such a topological description of the system bears no direct information on how quickly the vehicle speed goes to zero as a particular trajectory is traversed in the  $(u, \mathbf{s})$  state space, nor on the speed at which that trajectory evolves according to the equations of motion, it does clearly exhibit the regions of stable and unstable braking in terms of front and rear wheel slip. Some information on how the vehicle decelerates (or whether it decelerates) can be extracted, however, by quantifying steady-slip solutions: that is, the invariant manifolds in the  $(u, \mathbf{s})$  space.

For nonzero  $u$  and a pair of constant front and rear slip values, denoted  $\mathbf{s}^* = (s_r^*, s_f^*)$ , it follows that  $\mathbf{h}_b(\mathbf{s}^*) = (h_{br}(\mathbf{s}^*), h_{bf}(\mathbf{s}^*)) = (0, 0)$ . Thus, by inspection of

Equation (4.5), the time rate of change of slip in each wheel is identically equal to zero and remains constant, independent of vehicle speed. Correspondingly, the vehicle acceleration  $\dot{u} = -g(\Lambda_b(\mathbf{s}^*) \cos \theta - \sin \theta)$  is constant and the vehicle speed monotonically decreases to zero or increases—depending on the angle  $\theta$  and the magnitude of  $\Lambda_b(\mathbf{s}^*)$ —according to the equation

$$u(t) = u_o - (\Lambda_b(\mathbf{s}^*) \cos \theta - \sin \theta) gt, \quad u > 0, \quad t_f > t \geq 0, \quad (4.9)$$

where  $u_o$  is the vehicle speed at  $t = 0$ .

All combinations of  $\mathbf{s}^*$ , if they exist, define invariant sets of the two-wheel system. In order to quantify these steady-slip pairs, it is convenient to define the following sets:

$$\mathcal{S}_i^\pm = \{\mathbf{s} \mid h_{bi}(\mathbf{s}) = 0, h'_{bi}(\mathbf{s}) \lessgtr 0\}, \quad i = r, f.$$

$\mathcal{S}_r^+$  and  $\mathcal{S}_r^-$  are sets of all slip pairs  $\mathbf{s} = (s_r, s_f)$  such that the surfaces  $h_{br}(\mathbf{s})$  and  $h_{bf}(\mathbf{s})$  intersect the plane  $h_b(\mathbf{s}) = 0$  with negative and positive slopes, respectively, in the  $s_r$ -direction. The sets  $\mathcal{S}_f^+$  and  $\mathcal{S}_f^-$  are similarly defined in terms of slope along the  $s_f$ -axis. Figure 4.4a shows an example plot of these sets for  $\Upsilon_{br} = 3.5$ ,  $\Upsilon_{bf} = 10.0$ ,  $\theta = 0$ , and a particular vehicle geometry. The invariant sets of the two-wheel system and their stability types are determined in terms of  $\mathcal{S}_i^\pm$  ( $i = r, f$ ) and are defined as follows:

$$\begin{aligned} \mathbf{s}^+ &= \mathcal{S}_r^+ \cap \mathcal{S}_f^+ && \text{Stable Node} \\ \mathbf{s}^- &= \mathcal{S}_r^- \cap \mathcal{S}_f^- && \text{Unstable Node} \\ \mathbf{s}^\pm &= \mathcal{S}_r^+ \cap \mathcal{S}_f^- && \text{Saddle} \\ \mathbf{s}^\mp &= \mathcal{S}_r^- \cap \mathcal{S}_f^+ && \text{Saddle} \end{aligned}$$

The corresponding invariant manifolds of the two-wheel braking model are defined in

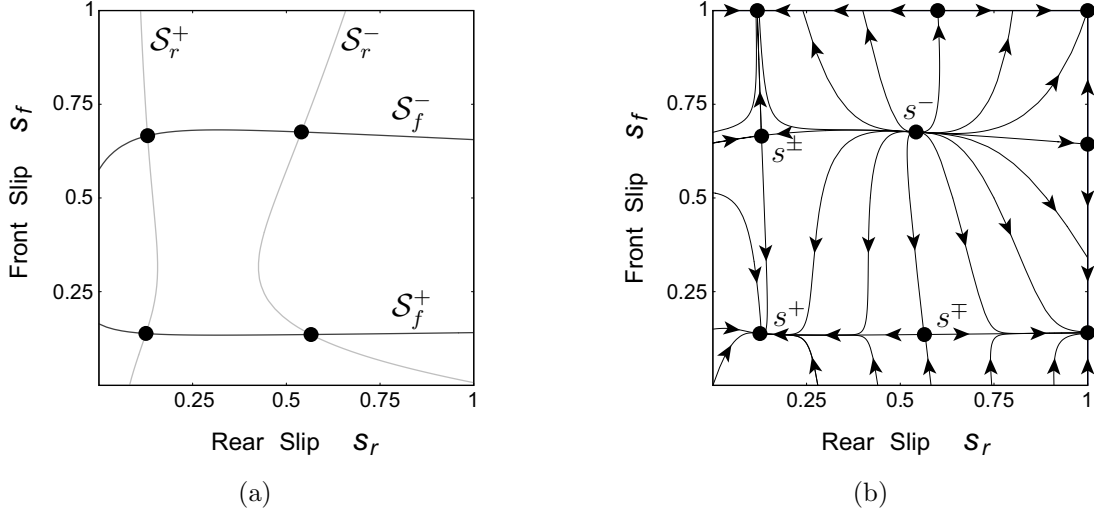


Figure 4.4. (a) The solution sets  $\mathcal{S}_i^\pm$  ( $i = r, f$ ) and (b) the corresponding state space description of the slip dynamics of the two-wheel model for  $h = 1.25$ ,  $c = 6$ ,  $b = 4$ ,  $\theta = 0$ ,  $\Psi = 15$ , and  $\Upsilon_{br} = 3.5$ ,  $\Upsilon_{bf} = 10.0$ .

terms of these invariant sets as

$$\mathcal{V}_b^* = \{(u, \mathbf{s}) \mid u > 0, \mathbf{s} = \mathbf{s}^*\}.$$

Since wheel slip is restricted in the plane such that  $\mathbf{s} \in I \times I$ ,

$$\mathcal{V}_{bi}^L = \{(u, \mathbf{s}) \mid u > 0, s_i = 1\}, \quad i = r, f \quad (4.10)$$

are also invariant manifolds, where, recall,  $L$  denotes lockup. Figure 4.4b shows an example state space description of the two-wheel model slip dynamics, indicating the steady-slip values  $\mathbf{s} = \mathbf{s}^*$  and their stability type as well as steady-slip values at wheel lockup. Depending on the relative values of  $\Upsilon_{br}$  and  $\Upsilon_{bf}$  there may be between zero and four such invariant points  $\mathbf{s}^*$  in the  $\mathbf{s}$ -plane.

### 4.1.3 Global Features of the Two-Wheel Braking Model

Depicted in Figure 4.5 is a qualitative description of the possible operating regimes—stable, mixed, or lockup—of the two-wheel model in braking as a function of the front and rear brake torques. The front brake torque  $\Upsilon_{bf}$  is defined along the ordinate, while the rear brake torque  $\Upsilon_{br}$  is defined along the abscissa. Here, "stable" implies that all trajectories tend toward a stable invariant set  $\mathbf{s}^*$  and the system experiences stable braking. "Mixed" regions indicate the possibility of either front or rear wheel lockup, but not both. Finally, "lockup" implies that  $s_f = 1$  and/or  $s_r = 1$  such that one or both wheels are locked.

In the *stable* region, which is indicated by the roman numeral *I*, there is a single stable invariant set and all initial slip conditions yield stable braking. In the *mixed (front)* region, denoted by *II*, the front wheel can tend to lockup—depending on the front brake torque—while the rear wheel experiences stable braking conditions. Similarly in region *III (mixed [rear])*, the rear wheel can tend to lockup—depending on the rear brake torque—while the front wheel experiences stable braking conditions. The *mixed (front & rear)* region, denoted by *IV*, indicates lockup conditions for either the front or rear wheel, or both. Region *V* is characterized by wheel lockup, where at most one wheel experiences stable braking. There are various subregions within region *V*, but the determination of these various regimes of lockup is left for future work. In Figure 4.5, the shaded regions indicate complicated bifurcation sequences that occur over small brake torque ranges. Example phase plane plots showing the slip dynamics of the system in each operating regime are also shown in Figure 4.5. Front slip is defined along the ordinate, while rear slip is defined along the abscissa.

As with the single-wheel braking model, the dynamic behavior of the two-wheel system in braking is completely determined by, in this case, the two functions  $h_{br}(\mathbf{s})$  and  $h_{bf}(\mathbf{s})$ . For a particular set of dimensionless brake torques, one need only find

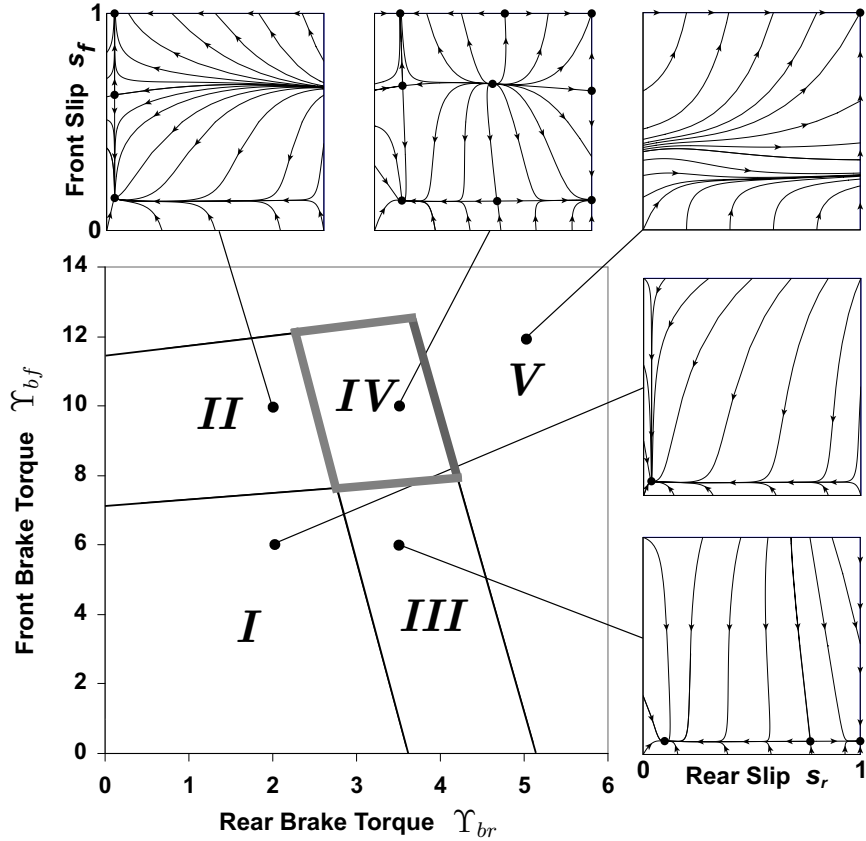


Figure 4.5. Qualitative description of the steady-slip conditions for the two-wheel braking model as a function of the brake torques ( $h = 2m$ ,  $c = 6m$ ,  $b = 4m$ ,  $\theta = 0$ , and  $\Psi = 15$ ): (I) *Stable*; (II) *Mixed (Front)*; (III) *Mixed (Rear)*; (IV) *Mixed (Front & Rear)*; (V) *Lockup*. Example slip space vector fields in front and rear slip.

the slip pairs  $\mathbf{s}^* = (s_r^*, s_f^*)$  that make both  $h_{br}(\mathbf{s})$  and  $h_{bf}(\mathbf{s})$  vanish identically, along with the gradients of each of these functions in the  $s_r$ - and  $s_f$ -directions, respectively. With this knowledge, a qualitative description of the slip dynamics can be constructed for the front and rear brake torque combination of interest. Figure 4.5 captures the essence of the possible operating regimes. There is much left for consideration, however; this is left for future work.

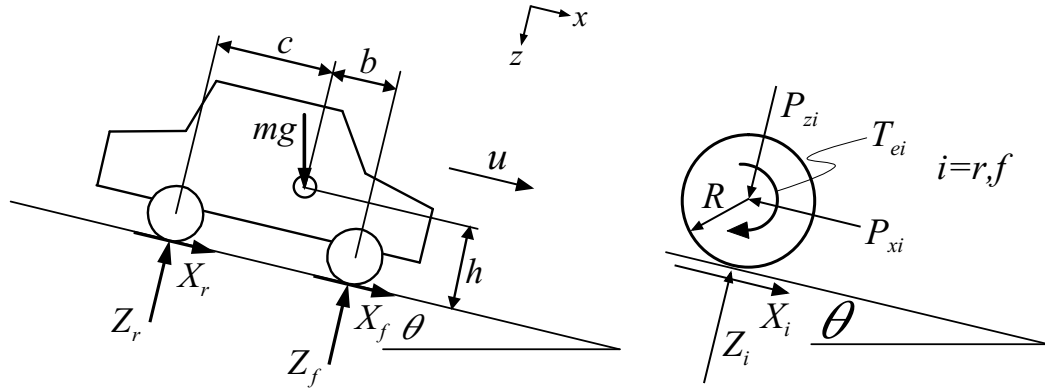


Figure 4.6. Schematic of the two-wheel vehicle acceleration model and corresponding free body diagram of a single wheel

## 4.2 The Two-Wheel Acceleration Model

A two-wheel vehicle acceleration model is shown schematically in Figure 4.6. It is identical to the two-wheel braking model of Section 4.1, except in the direction of the front and rear wheel torques and longitudinal forces. Here, the model is developed, and an analysis similar to that of the two-wheel braking model is motivated, but an investigation of the dynamics is not pursued.

The equations of motion are developed in the same way as the two-wheel vehicle braking model of Section 4.1. Rear and front wheel slip are determined by Equation (4.2), with  $\omega_i R > u$  ( $i = r, f$ ), and the longitudinal acceleration forces  $X_i$  ( $i = r, f$ ) are defined in terms of the friction law given by Equation (4.1).

### 4.2.1 Equations of Motion

The two-wheel acceleration model is formulated in terms of the dynamic states  $u$ ,  $s_r$ , and  $s_f$ . Rear and front longitudinal braking forces and wheel slip are, respectively, defined by Equation (4.1) and Equation (4.2). The system dynamics are then

governed by

$$\left. \begin{aligned} \dot{u} &= g(\Lambda_t(\mathbf{s}) \cos \theta + \sin \theta) \\ \dot{\mathbf{s}} &= \frac{g}{u} \mathbf{h}_t(\mathbf{s}) \end{aligned} \right\}, \quad \omega_i R > 0 \quad (i = r, f), \quad \mathbf{s} \in -I \times -I, \quad (4.11)$$

where  $\mathbf{s} = (s_r, s_f)$  and  $\mathbf{h}_t(\mathbf{s}) = (h_{tr}(\mathbf{s}), h_{tf}(\mathbf{s}))$  are vectors. The function

$$\Lambda_t(\mathbf{s}) = \frac{\mu(s_r) \frac{b}{l} + \mu(s_f) \frac{c}{l}}{1 - \frac{b}{l} (\mu(s_r) - \mu(s_f))}$$

is nondimensional and is a measure of the vehicle acceleration along the road surface.

The functions

$$h_{ti}(\mathbf{s}) = (s_i + 1)^2 [(s_i + 1)^{-1} (\Lambda_t(\mathbf{s}) \cos \theta + \sin \theta) + \Psi \mu(s_i) \lambda(\mathbf{s}) - \Upsilon_{ei}], \quad i = r, f \quad (4.12)$$

are dimensionless, where  $\Upsilon_{ei} = \frac{R}{Jg} T_{ei}$  ( $i = r, f$ ) are the rear and front dimensionless engine torques, and  $\lambda_i$  ( $i = r, f$ ) are the nondimensional dynamic normal loads on the rear and front wheels given by Equation (4.7). Since  $\frac{ds_r}{ds_f} = \frac{h_{tr}(\mathbf{s})}{h_{tf}(\mathbf{s})}$ , invariant sets can be defined similarly to the two-wheel braking analysis and a qualitative description of the steady-slip conditions could be obtained similar to Figure (4.5). This is left for future work.

# CHAPTER 5

## Conclusions and Directions for Future Work

The results presented here offer new insight into the behavior of vehicles during longitudinal braking and acceleration. In each case considered, the unique features of the modeling approach allow one to capture the full range of dynamic behavior of single- and two-wheel models in a simple geometrical manner. By choosing the forward vehicle speed and longitudinal wheel slip as dynamics states, the dynamic equations of motion for the single- and two-wheel traction models lend themselves to a relatively simple investigation and interpretation using the tools from nonlinear dynamics. This choice of dynamic states, where wheel slip plays a central role, allows the dynamics for the entire range of vehicle speeds and slip values to be captured by a single function for the single-wheel model and two functions for the two-wheel model. These functions completely describe the tractive behavior of a given vehicle in terms of slip and the brake or engine torque. The relative simplicity of the analyses described herein is a consequence of the choice of dynamic states and the interpretation of the resulting equations of motion.

Perhaps the most important conclusion from this work is the fact that the lockup instability in the single-wheel model does not occur when the brake torque leads to

the maximum point on the slip curve but at a lower brake torque. The traditional assumption—that attaining the maximum coefficient of friction leads to lockup—is shown to be an approximation that is accurate only when the ratio of the tire/wheel inertia is small compared to the vehicle inertia. Since this ratio is typically small, the approximation is quite good. However, when considering a light vehicle with relatively large tire/wheel inertia, the approximation becomes less accurate. In either case, it is of interest to note that the commonly held view of lockup is only an approximation.

This analysis is the first step in a new direction for the modeling of braking dynamics, and much remains to be done. Some lines of future work include the following:

- more detailed parameter studies for specific vehicles under various road conditions.
- use of the two-wheel braking model to assess brake proportioning strategies wherein torques are independently assigned to the front and rear wheels.
- a more thorough study of the two-wheel acceleration model.
- the effects of cornering on braking and acceleration, wherein a four-wheel model would be required.
- the incorporation of these models into ABS/TCS development, where slip plays a central role.

# BIBLIOGRAPHY

## BIBLIOGRAPHY

- [1] T. Gillespie, *Fundamentals of Vehicle Dynamics*. Society of Automotive Engineers (SAE), Inc, 1992.
- [2] J. Wong, *Theory of Ground Vehicles*. New York: John Wiley and Sons, 1978.
- [3] “Antilock brake system review,” *Society of Automotive Engineers (SAE)*, vol. 25, pp. 90–102, June 1992.
- [4] E. Bakker, L. Nyborg, and H. Pacejka, “Tyre modelling for use in vehicle dynamics studies,” *Society of Automotive Engineers*, vol. 2, no. 870421, pp. 190–204, 1987.
- [5] E. Bakker, H. Pacejka, and L. Lidner, “A new tire model with and application in vehicle dynamics studies,” *Society of Automotive Engineers*, no. 890087, pp. 101–113, 1989.
- [6] Y. Liu and J. Sun, “Target slip tracking using gain-scheduleing for antilock braking systems,” *Proceedings of the American Control Conference*, vol. 2, pp. 1178–1182, June 1995.
- [7] K. Kobayashi, K. C. Cheok, and K. Watanabe, “Estimation of absolute vehicle speed using fuzzy logic rule-based kalman filter,” *Proceedings of the American Control Conference*, vol. 5, pp. 3086–3090, June 1995.
- [8] G. Goodenow, T. Kolhoff, and F. Smithson, “Tire-road friction measuring system—a second generation,” *Society of Automotive Engineers*, no. 680137, pp. 571–579, 1968.
- [9] J. Harned, L. Johnston, and G. Scharpf, “Measurement of tire brake force characteristics as related to wheel slip (antilock) control system design,” *Society of Automotive Engineers*, no. 690214, pp. 909–925, 1969.

- [10] A. Sitchin, “Acquisition of transient tire force and moment data for dynamic vehicle handling simulations,” *Society of Automotive Engineers*, vol. 4, no. 831790, pp. 1098–1110, 1983.
- [11] J. Guckenheimer and P. Holmes, *Nonlinear Oscillations, Dynamical Systems, and Bifurcations of Vector Fields*, vol. 42 of *Applied Mathematical Sciences*. Springer-Verlag, 1983.